

Structured Bayesian variable selection for multiple correlated response variables and high-dimensional predictors

Zhi Zhao^{*1,2}, Marco Banterle³, Alex Lewin^{#3}, and Manuela Zucknick^{#1}

¹Oslo Centre for Biostatistics and Epidemiology, University of Oslo, Norway

²Department of Cancer Genetics, Institute for Cancer Research, Oslo University Hospital, Norway

³Department of Medical Statistics, London School of Hygiene & Tropical Medicine, UK

Abstract

It is becoming increasingly common to study complex associations between multiple phenotypes and high-dimensional genomic features in biomedicine. However, it requires flexible and efficient joint statistical models if there are correlations between multiple response variables and between high-dimensional predictors. We propose a structured multivariate Bayesian variable selection model to identify sparse predictors associated with multiple correlated response variables. The approach makes use of known structure information between the multiple response variables and high-dimensional predictors via a Markov random field (MRF) prior for the latent indicator variables of the coefficient matrix of a sparse seemingly unrelated regressions (SSUR). The structure information included in the MRF prior can improve the model performance (i.e., variable selection and response prediction) compared to other common priors. In addition, we employ random effects to capture heterogeneity of grouped samples. The proposed approach is validated by simulation studies and applied to a pharmacogenomic study which includes pharmacological profiling and multi-omics data (i.e., gene expression, copy number variation and mutation) from *in vitro* anti-cancer drug sensitivity screening.

Key words: Bayesian multivariate regression; seemingly unrelated regression; structured spike-and-slab prior; Markov random field prior, random effects.

*To whom correspondence should be addressed: zhi.zhao@medisin.uio.no. #These are joint last authors.

1 Introduction

Multivariate regression models involve multiple response variables, for example, expression quantitative trait loci (eQTL) analysis and analysis of large-scale drug sensitivity screening datasets have multiple correlated response variables and high-dimensional predictors. A fundamental task is to study the structures or associations in the integrative datasets via joint statistical models.

In this work, we analyze data from the Genomics of Drug Sensitivity in Cancer (GDSC) database (Garnett et al., 2012; Yang et al., 2013), which contains the results from drug sensitivity screens to hundreds of cancer drugs for hundreds of cancer cell lines and multi-omics characterisation of these cell lines. The large-scale *in vitro* cancer drug screens produced a large amount of drug sensitivity data which are expected to be correlated for drugs that have similar mechanisms of action or common target genes or pathways. Meanwhile, the genomic information, including genome-wide measurements of mRNA expression, DNA copy numbers and DNA mutations, for cancer cell lines was measured, which is expected to guide personalized cancer therapies through prediction of drug sensitivity (Garnett et al., 2012; Barretina et al., 2012; Pemovska et al., 2013; Gray and Mills, 2015). Since multiple omics characterizations reflect different aspects of information of the same system or co-functionality of multiple gene features (Kim et al., 2019), an analysis of joint associations between the correlated multiple phenotypes (e.g. multiple drugs) and high-dimensional molecular features (i.e., multi-omics data) is desired, but poses both theoretical and computational challenges.

It is both computationally expensive to learn a covariance structure of multiple response variables and to sample a fully enumerated model space for high-dimensional predictors. Bayesian modelling provides flexibility to specify the relationships in such complex data. Richardson et al. (2011) proposed hierarchical related regressions (HRR) by assuming independent residuals (i.e., independent residual priors), which can induce correlations to the posteriors of responses. (Ando and Zellner, 2010; Holmes et al., 2002; Deshpande et al., 2019). Petretto et al. (2010) proposed Sparse Bayesian Regression models and showed an inverse Wishart prior for the covariance matrix of residuals. Furthermore, a hyper-inverse Wishart prior can be used to learn a sparse graph structure for the covariance matrix of high-dimensional variables (Carvalho et al., 2007; Wang, 2010; Bhadra and Mallick, 2013), thus performing covariance selection. Bottolo et al. (2021) presented a Bayesian sparse seemingly unrelated regressions (SSUR) model to learn a sparse structure of the covariance matrix of high-dimensional response variables by assuming an underlying decomposable graph between response variables.

Besides imposing different structures on a covariance matrix via the choice of priors, it is necessary to impose variable selection priors for high-dimensional predictors simultaneously. Jia and Xu (2007) used a spike-and-slab prior and hyper predictor-effect prior for mapping each genetic marker to multiple phenotypes (i.e., eQTL). Bottolo et al. (2011) proposed a hotspot detection prior for variable selection in multivariate regressions, which decomposes the association probability to a predictor and response effect. Lee et al. (2017) utilized a Markov random field (MRF) prior to encourage the joint selection of the same predictor across several correlated response variables. The Bayesian SSUR model (Bottolo et al., 2021) also performs variable selection of high-dimensional predictors by independent spike-and-slab priors.

For computational challenges, the HRR model and Bayesian SSUR model apply an Evolutionary Stochastic Search (ESS) algorithm based on Evolutionary Monte Carlo (Bottolo and Richardson, 2010) for posterior inference of high-dimensional regression coefficients. Ando and Zellner (2010) combined a Direct Monte Carlo approach and an importance sampler for the estimation of the SUR model but only in low-dimensional settings.

In this article, we propose a structured Bayesian variable selection approach based on the Bayesian SSUR model. The proposed approach employs an MRF prior for the latent indicator variables of the regression matrix to emphasize a joint structure between high-dimensional predictors of multiple response variables. This joint structure represents known associations between predictor variables, between response variables, and between predictors and responses. For example, Figure 1 illustrates two groups of drugs and their corresponding two groups of target genes or pathways across multiple omics characterizations. When using omics data to predict drug responses, the associations between the multiples drugs and omics features can include prior knowledge about the two groups of drugs and their target genes or target pathways. An MRF prior is able to address the joint structure by adding the edges for omics features within a group of target genes or pathways that correspond to the group of their targeting drugs. In addition, if the drug responses are measured on cell lines from different cancer types or different tissues, we use random effects to capture the sample heterogeneity arising from these sample groups. An R package BayesSUR (Zhao et al., 2021) is available from the Comprehensive R Archive Network at <http://CRAN.R-project.org/package=BayesSUR>.

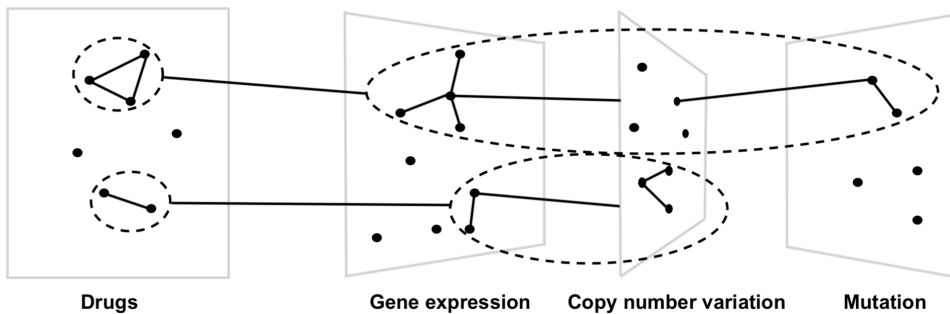


Figure 1: Illustration of the drug groups and omics path (adapted from Ruffieux (2019)).

The rest of the article is organized as follows. In Section 2, we first introduce the Bayesian SSUR model. Then we propose an MRF prior for the latent indicator variables of the coefficient matrix, and random effects for the regression coefficients of sample group variables. Section 3 compares the performances of Bayesian SSUR model with our MRF prior to that of a model using the hotspot prior developed by Bottolo et al. (2011) with respect to structure recovery and prediction in simulated data sets. In Section 4, we analyse a dataset from the GDSC database. In Section 5, we conclude the article with a discussion.

2 Methodology

2.1 SSUR model

We study a multivariate regression model with a response matrix $\mathbf{Y}_{n \times m}$ from n samples and m response variables. All response variables are regressed on the same p predictors which are measured on the n samples, so that the predictor matrix is $\mathbf{X}_{n \times p}$. Associations between the responses \mathbf{Y} and predictors \mathbf{X} are captured by a coefficient matrix $\mathbf{B}_{p \times m}$. We first assume correlated response variables, but independent samples. Section 2.3 will then extend the model to allow for correlated samples. The classic SUR model is defined as

$$\begin{aligned} \mathbf{Y} &= \mathbf{X}\mathbf{B} + \mathbf{U}, \\ \text{vec}\{\mathbf{U}\} &\sim \mathcal{N}(\mathbf{0}, \Psi \otimes \mathbb{I}_n), \end{aligned} \tag{1}$$

where the residuals have correlated columns with covariance Ψ and independent rows, and $\text{vec}\{\cdot\}$ is to vectorize a matrix by column.

In the Bayesian framework, to efficiently sample from the posterior distribution of the regression coefficients from (1), Zellner and Ando (2010) reparametrized the SUR model and proposed

a direct Monte Carlo procedure. Bottolo et al. (2021) used the same reparametrization for the SUR model, but with an inverse Wishart prior $\Psi \sim \mathcal{IW}(\nu, \tau \mathbb{I}_m)$. Briefly, then model (1) can be rewritten as

$$\begin{aligned} \mathbf{y}_j &= \mathbf{X}\boldsymbol{\beta}_j + \sum_{l < j} \mathbf{u}_l \rho_{jl} + \boldsymbol{\epsilon}_j, \quad j = 1, \dots, m, \\ \boldsymbol{\epsilon}_j &\sim \mathcal{N}(\mathbf{0}, \sigma_j^2 \mathbb{I}_n), \end{aligned} \tag{2}$$

where $\mathbf{u}_l = \mathbf{y}_l - \mathbf{X}\boldsymbol{\beta}_l$. The reparametrized parameters (σ_j^2, ρ_{jl}) have priors

$$\begin{aligned} \sigma_j^2 &\sim \mathcal{IG}\left(\frac{\nu - m + 2j - 1}{2}, \frac{\tau}{2}\right), \\ \rho_{jl} | \sigma_j^2 &\sim \mathcal{N}\left(0, \frac{\sigma_j^2}{\tau}\right), j > l, \end{aligned} \tag{3}$$

where ν is fixed and $\tau \sim \mathcal{Gamma}(a_\tau, b_\tau)$. Note that the joint distribution $f(\mathbf{Y}|\mathbf{X}, \mathbf{B}, \Psi)$ is the same regardless of the order used for the decomposition since we are simply factorising it by chain-conditioning (Bottolo et al., 2021).

The reparametrization makes parallel computation of the likelihood across multiple response variables possible, which especially benefits high-dimensional response variables. If only a few of the p predictor variables are assumed to be associated with any of the response variables, we use a latent indicator matrix $\boldsymbol{\Gamma} = \{\gamma_{kj}\}$ for variable selection. If $\gamma_{kj} = 1$, then $\beta_{kj} \neq 0$ and the k th predictor is regarded as an associated predictor to the j th response variable; otherwise $\gamma_{kj} = 0$ and $\beta_{kj} = 0$. Independent spike-and-slab priors (George and McCulloch, 1993; Brown et al., 1998) for the regression coefficients can be used to find a small subset of predictors that explains the variability of \mathbf{Y} , for example:

$$\beta_{kj} | \gamma_{kj}, w \sim \gamma_{kj} \mathcal{N}(0, w) + (1 - \gamma_{kj}) \delta_0(\beta_{kj}), \tag{4}$$

where $w \sim \mathcal{IG}(a_w, b_w)$ and $\delta_0(\cdot)$ is the Dirac delta function.

We may not only introduce sparsity to the high-dimensional coefficient matrix, but also sparsity to the precision matrix Ψ^{-1} , which implies that the residuals $\mathbf{u}_l = \mathbf{y}_l - \mathbf{X}\boldsymbol{\beta}_l$ and $\mathbf{u}_j = \mathbf{y}_j - \mathbf{X}\boldsymbol{\beta}_j$ for only a few pairs of response variables $l \neq j$ have non-zero partial correlations, assuming a multivariate normal distribution for the residuals. Such a sparse precision matrix can be conceptualized as a graph \mathcal{G} , with nodes representing the residual variables \mathbf{u}_l , and edges between them corresponding to non-zero elements of the precision matrix. Bottolo et al. (2021)

suggested a hyper-inverse Wishart prior for Ψ instead of an inverse Wishart prior, i.e.,

$$\Psi \sim \mathcal{HIW}_{\mathcal{G}}(\nu, \tau \mathbb{I}_m). \quad (5)$$

It assumes an underlying decomposable graph \mathcal{G} between residuals. The HIW prior on decomposable graphs greatly enhances computational power since the parameters are updated within each clique and there is no computationally expensive normalisation constant to calculate. Since the fully Bayesian estimation procedure produces edges averaged over many different graphs, the posterior mean graph can well approximate non-decomposable graphs (Fitch et al., 2014). A sparse graph \mathcal{G} can result in sparse Ψ^{-1} . So Bottolo et al. (2021) specified a *Bernoulli*(η) prior for each edge of the graph. Then a Binomial prior is on the cardinality edge-set

$$|\mathcal{E}| \sim \mathcal{Binomial}(m(m-1)/2, \eta), \quad (6)$$

where $\eta \sim \mathcal{Beta}(a_\eta, b_\eta)$ controls the sparsity of the graph. Based on (5) and (6), the parameters σ^2 and ρ are indexed across the response variables of each clique of \mathcal{G} rather than all response variables.

In addition to sparse covariance selection, Bottolo et al. (2021) also proposed sparse variable selection for the predictor variables via a hotspot prior (i.e., a multiplicative prior) for the hyper-parameter ω_{kj} in $\gamma_{kj} \sim \mathcal{Ber}(\omega_{kj})$.

Prior specification

For the hyper-parameters ν and τ in $\Psi \sim \mathcal{HIW}_{\mathcal{G}}(\nu, \tau \mathbb{I}_m)$, we specify a fixed $\nu = m + 2$ and $\tau \sim \mathcal{Gamma}(a_\tau, b_\tau)$. $\nu = m + 2$ is suggested by Bottolo et al. (2021), because it is the smallest integer degree resulting in a proper prior for the reparametrized parameter σ_j^2 . A sensitivity analysis for these hyper-parameters of the hyper-inverse Wishart prior can be found in Supplementary S4.

The hyper-parameters a_w and b_w control the variance of the spike-and-slab prior for non-zero regression coefficients in (4), which determines the posterior scale for the estimated effects. In order to provide a sufficiently large scale for the effects, we would like to allow some posterior density for values of w that will correspond to non-negligible posterior density for values of β_{kj} larger than the upper 95% confidence bound $\mathbb{E}[\beta_{kj}] + 1.96\sqrt{\text{Var}[\beta_{kj}]}$, where $\mathbb{E}[\cdot]$ and $\text{Var}[\cdot]$ are the mean and variance of the prior for the effect β_{kj} . This is to ensure that prior of w provides

large enough variation to be able to cover a wide range of β_{kj} . Since w has posterior conditional

$$w|a_w, b_w, \mathbf{\Gamma}, \mathbf{B} \sim \mathcal{IG} \left(a_w + \frac{1}{2} \sum_{kj} \gamma_{kj}, b_w + \frac{1}{2} \sum_{k,j} \beta_{kj}^2 \right), \quad (7)$$

we can choose proper a_w and b_w according to this posterior conditional with 5% quantile larger than $\mathbb{E}[\beta_{kj}] + 1.96\sqrt{\text{Var}[\beta_{kj}]}$. Since a_w and b_w are combined with the factors $\frac{1}{2} \sum_{kj} \gamma_{kj}$ and $\frac{1}{2} \sum_{kj} \beta_{kj}^2$ respectively, a_w and b_w can be chosen with similar scales as the two factors.

For example, we assume a model sparsity (i.e., proportion of nonzero coefficients) $r_{sparsity} = \frac{1}{mp} \sum_{kj} \gamma_{kj} \in (0, 1)$, and $\mathbb{E}[\beta_{kj}]$ and $\text{Var}[\beta_{kj}]$ can either be estimated roughly from previous studies or elucidated using expert knowledge about typical effect sizes in similar studies. Then we specify

$$\begin{aligned} a_w &= \text{const}_a \cdot 1/2 \cdot m \cdot p \cdot r_{sparsity}, \\ b_w &= \text{const}_b \cdot 1/2 \cdot m \cdot p \cdot r_{sparsity} \cdot (\mathbb{E}[\beta_{kj}])^2, \end{aligned}$$

where const_a and const_b are chosen to ensure that the 5% quantile of the posterior conditional (7) is larger than $\mathbb{E}[\beta_{kj}] + 1.96\sqrt{\text{Var}[\beta_{kj}]}$.

2.2 SSUR model with MRF prior

Figure 1 illustrates possible known relationships between the drug responses and genomic predictors. As an example, we can imagine a group of drugs with the same mechanism of action, where the response of a cancer cell to these drugs depends on a certain gene to be silenced. Gene silencing can either occur via a genomic alteration such as a deletion event or missense mutation, or via another downregulation of gene expression. Such gene silencing might therefore be observable in one or several omics data sources, e.g. in gene expression, copy number variation or mutation data. We may include such prior knowledge on the regression coefficient matrix in the SUR model (1), instead of using independent or hotspot priors (Richardson et al., 2011; Lewin et al., 2016; Bottolo et al., 2021). We propose to use an MRF prior for the latent indicator vector $\gamma = \text{vec}\{\mathbf{\Gamma}\}$ to address a prior structure for the associations between the response variables and predictors. The MRF prior is

$$f(\gamma|d, e, G) \propto \exp\{d\mathbf{1}^\top \gamma + e\gamma^\top G\gamma\}, \quad (8)$$

where the scalar d controls the overall model sparsity, scalar e determines the strength of the structure relationships between responses and predictors, and G is an $mp \times mp$ (possibly weighted) adjacency matrix representing a graph to include prior structure knowledge. The term $d\mathbb{1}^\top \boldsymbol{\gamma}$ in (8) can be generalized to $\mathbf{d}^\top \boldsymbol{\gamma}$, where the vector \mathbf{d} will assign different relative contributions to the prior selection probabilities of the predictors. In the G matrix, we assign a positive edge potential $\{k + j(p - 1), k' + j'(p - 1)\}$ -element if the latent indicator variables γ_{kj} and $\gamma_{k'j'}$ are correlated. To illustrate the idea, we consider a simple case with three response variables (i.e., \mathbf{y}_1 , \mathbf{y}_2 and \mathbf{y}_3) and four predictors (i.e., \mathbf{x}_1 , \mathbf{x}_2 , \mathbf{x}_3 and \mathbf{x}_4). When the predictors \mathbf{x}_1 and \mathbf{x}_2 are assumed *a priori* to be associated with responses \mathbf{y}_1 and \mathbf{y}_2 , and \mathbf{x}_3 and \mathbf{x}_4 are assumed to be associated with \mathbf{y}_3 , then G is a 12×12 matrix given by

$$G = \begin{matrix} & \begin{matrix} \gamma_{11} & \gamma_{21} & \gamma_{31} & \gamma_{41} & \gamma_{12} & \gamma_{22} & \gamma_{32} & \gamma_{42} & \gamma_{13} & \gamma_{23} & \gamma_{33} & \gamma_{43} \end{matrix} \\ \begin{matrix} \gamma_{11} \\ \gamma_{21} \\ \gamma_{31} \\ \gamma_{41} \\ \gamma_{12} \\ \gamma_{22} \\ \gamma_{32} \\ \gamma_{42} \\ \gamma_{13} \\ \gamma_{23} \\ \gamma_{33} \\ \gamma_{43} \end{matrix} & \begin{pmatrix} 0 & 1 & 0 & 0 & 1 & 1 & 0 & 0 & 0 & 0 & 0 & 0 \\ 1 & 0 & 0 & 0 & 1 & 1 & 0 & 0 & 0 & 0 & 0 & 0 \\ 0 & 0 & 0 & 0 & 0 & 0 & 0 & 0 & 0 & 0 & 0 & 0 \\ 0 & 0 & 0 & 0 & 0 & 0 & 0 & 0 & 0 & 0 & 0 & 0 \\ 1 & 1 & 0 & 0 & 0 & 1 & 0 & 0 & 0 & 0 & 0 & 0 \\ 1 & 1 & 0 & 0 & 1 & 0 & 0 & 0 & 0 & 0 & 0 & 0 \\ 0 & 0 & 0 & 0 & 0 & 0 & 0 & 0 & 0 & 0 & 0 & 0 \\ 0 & 0 & 0 & 0 & 0 & 0 & 0 & 0 & 0 & 0 & 0 & 0 \\ 0 & 0 & 0 & 0 & 0 & 0 & 0 & 0 & 0 & 0 & 0 & 0 \\ 0 & 0 & 0 & 0 & 0 & 0 & 0 & 0 & 0 & 0 & 0 & 1 \\ 0 & 0 & 0 & 0 & 0 & 0 & 0 & 0 & 0 & 0 & 1 & 0 \end{pmatrix} \end{matrix}.$$

Any nonzero element in G above can be any positive number which indicates a weight for the prior relationship between two latent indicator variables. Here for simplicity, we construct a symmetric G matrix and assume all nonzero weights to be 1. If one only knows or assumes relationships among response variables and relationships among predictors, but not between responses and predictors, then $G = G_y \otimes G_x - \mathbb{I}_{mp}$. Here we use $-\mathbb{I}_{mp}$ to only allow zero diagonals in G , because nonzero diagonals can be captured by the term $d\mathbb{1}^\top \boldsymbol{\gamma}$. For example, if we know predictors \mathbf{x}_1 and \mathbf{x}_2 are related, \mathbf{x}_3 and \mathbf{x}_4 are related, but do not have any information about three response variables, then $G = G_y \otimes G_x - \mathbb{I}_{12}$ where $G_y = \mathbb{I}_3$ and

$$G_x = \begin{pmatrix} 1 & 1 & 0 & 0 \\ 1 & 1 & 0 & 0 \\ 0 & 0 & 1 & 1 \\ 0 & 0 & 1 & 1 \end{pmatrix}.$$

Prior specification

It is known that the hyper-parameter e in (8) can display a phase transition behaviour (Li and Zhang, 2010; Stingo et al., 2011) which results in a sharp increase in the number of selected predictors (i.e., $\beta_{kj} \neq 0$) with a small change of e given a value (w, d) . In the MRF prior (8), the model sparsity is $\text{logit}^{-1}d$ which can be used to specify the hyper-parameter d . Here logit is log-odds that is the natural logarithm of the odds. Hyper-parameter w in the spike-and-slab prior (4) can be specified by the guidance in Section 2.1. To specify e , Stingo et al. (2011); Lee et al. (2017) first looked for the phase transition boundary, and then implemented a grid search for the hyper-parameter. This might still search many values for e over the phase transition boundary, which would result in very dense models in high-dimensional settings. So we first determine the expected largest value e to avoid searching in the space of too dense models which would be computationally slow, and then implement the grid search strategy. If one wants to specify model sparsity in the range (c_1, c_2) , one can achieve this by specifying the hyper-parameter d subject to $\text{logit}^{-1}d = c_1$ and search hyper-parameter e from 0 to $-d - \ln(c_2^{-1} - 1)$. Because of $d = \text{logit}^{-1}c_1$, c_1 represents a lower bound for the model sparsity which is reached if $e = 0$. A rough estimate for $e \geq 0$ is given by $-d - \ln(c_2^{-1} - 1)$ based on the assumed largest sparsity c_2 (see Supplementary S1).

2.3 SSUR model with MRF prior and random effects

The SSUR model with hotspot prior in Section 2.1 and SSUR model with MRF prior in Section 2.2 both assume independent and identically distributed samples conditional on the predictors. However, samples can be heterogeneous, especially in applications with large sample size. For example, large-scale drug screens may include cell line samples from different cancer tissue types. We address the heterogeneity of multiple sample groups by introducing random effects into the model.

Let $\mathbf{Z}_{n \times T}$ be indicator variables representing n samples from T heterogeneous groups. We define an SUR model which includes spike-and-slab priors (4), hyper-inverse Wishart prior (5),

MRF prior (8) and random effects:

$$\begin{aligned}
\mathbf{Y} &= \mathbf{Z}\mathbf{B}_0 + \mathbf{X}\mathbf{B} + \mathbf{U}, \\
\beta_{0,tj}|w_0 &\sim \mathcal{N}(0, w_0), \\
\beta_{kj}|\gamma_{kj}, w &\sim \gamma_{kj}\mathcal{N}(0, w) + (1 - \gamma_{kj})\delta_0(\beta_{kj}), \\
w_0 &\sim \mathcal{IG}(a_{w_0}, b_{w_0}), \\
w &\sim \mathcal{IG}(a_w, b_w), \\
\gamma|d, e, G &\propto \exp\{d\mathbb{1}^\top\gamma + e\gamma^\top G\gamma\}, \\
\text{vec}\{\mathbf{U}\} &\sim \mathcal{N}(\mathbf{0}, \Psi \otimes \mathbb{I}_n), \\
\Psi &\sim \mathcal{HTWG}(\nu, \tau\mathbb{I}_m), \\
\tau &\sim \mathcal{Gamma}(a_\tau, b_\tau),
\end{aligned} \tag{9}$$

where the random effects $\mathbf{B}_0 = \{\beta_{0,tj} : t = 1, \dots, T; j = 1, \dots, m\}$, and all priors above are mutually independent.

Let us look into details of the random effects. For any i th sample and j th response variable, we have

$$y_{ij} = x_i^\top \beta_j + z_i^\top \beta_{0,j} + u_{ij}.$$

For the i th sample, the covariance between the j th and j' th response variables is $\psi_{jj'}$ that is the jj' -element of Ψ , since

$$\text{Cov}[y_{ij}, y_{ij'}] = \text{Cov}[x_i^\top \beta_j + z_i^\top \beta_{0,j} + u_{ij}, x_i^\top \beta_{j'} + z_i^\top \beta_{0,j'} + u_{ij'}] = \text{Cov}[u_{ij}, u_{ij'}] = \psi_{jj'}.$$

Although the priors for the coefficients \mathbf{B}_0 and \mathbf{B} in (9) do not provide any correlation between different responses for the same sample, the hyper-inverse Wishart prior on Ψ models correlations between the response variables, and so does an inverse Wishart prior on Ψ . If we look at the reparametrization (3) from the inverse Wishart prior, or similarly from the hyper-inverse Wishart prior, correlations between the response variables are contained in the reparametrized parameter $\boldsymbol{\rho}$.

For the j th response variable, the covariance between the i th and i' th samples is

$$\begin{aligned}\text{Cov}[y_{ij}, y_{i'j}] &= \text{Cov}[x_i^\top \boldsymbol{\beta}_j + z_i^\top \boldsymbol{\beta}_{0,j} + u_{ij}, x_{i'}^\top \boldsymbol{\beta}_j + z_{i'}^\top \boldsymbol{\beta}_{0,j} + u_{i'j}] \\ &= wx_i^\top x_{i'} + w_0 z_i^\top z_{i'}. \\ &= \begin{cases} wx_i^\top x_{i'}, & \text{if } i\text{th and } i'\text{th samples belong to different groups } (z_i \neq z_{i'}), \\ wx_i^\top x_{i'} + w_0, & \text{if } i\text{th and } i'\text{th samples belong to the same group } (z_i = z_{i'}), \end{cases}\end{aligned}$$

in which the hyper-parameter w_0 in the random effect determines the correlation between two samples from the same group.

Prior specification

We would like a weakly informative prior for $\beta_{0,tj}$ based on previous studies or expert knowledge in applications. In pharmacogenomic studies from multiple cancer tissues, for predict drug responses a tissue effect is usually stronger than a gene effect. Therefore it is appropriate to specify a larger hyper-parameter w_0 than w . Similar to the specification for the hyper-parameters a_w and b_w , we can choose appropriate a_{w_0} and b_{w_0} . But there is no variable selection for the random effects, i.e., $r_{sparsity} = 1$, and the random effects are centred at zero, i.e., $\mathbb{E}[\beta_{0,tj}] = 0$.

2.4 Posterior computation

Posterior inference for the SSUR model with the MRF prior with or without additional random effects can be done in a similar manner to Bottolo et al. (2021). For simplicity, here we describe the SUR model (2) with an inverse Wishart prior for the residual covariance matrix Ψ and an MRF prior for the latent indicator variables γ . Then the joint posterior distribution is

$$\begin{aligned}& f(\mathbf{B}, \boldsymbol{\Gamma}, w, \boldsymbol{\rho}, \boldsymbol{\sigma}^2, \tau | \mathbf{Y}, \mathbf{X}) \\ &= f(\mathbf{Y} | \mathbf{X}, \mathbf{B}, \boldsymbol{\rho}, \boldsymbol{\sigma}^2) f(\mathbf{B} | \boldsymbol{\Gamma}, w) f(\boldsymbol{\Gamma} | G, d, e) f(w) f(\boldsymbol{\rho} | \boldsymbol{\sigma}^2, \tau) f(\boldsymbol{\sigma}^2 | \tau) f(\tau) \\ &= \prod_j f(\mathbf{y}_j | \mathbf{X}, \mathbf{B}, \boldsymbol{\rho}, \boldsymbol{\sigma}^2) \prod_{k,j} f(\beta_{kj} | \gamma_{kj}, w) f(\boldsymbol{\gamma} | G, d, e) f(w) \prod_{j,l < j} f(\rho_{jl} | \sigma_j^2, \tau) \prod_j f(\sigma_j^2 | \tau) f(\tau),\end{aligned}\tag{10}$$

where $\boldsymbol{\rho}$ and $\boldsymbol{\sigma}^2$ are vectors of $\{\rho_{jl}\}$ and $\{\sigma_j^2\}$, respectively. Since $\mathbf{y}_j | \mathbf{X}, \mathbf{B}, \boldsymbol{\rho}, \boldsymbol{\sigma}^2$ is normally distributed with mean $\mathbf{X}\boldsymbol{\beta}_j + \sum_{l < j} \mathbf{u}_l \rho_{jl}$ and variance $\sigma_j^2 \mathbb{I}_n$, we can obtain the full conditional distributions of the regression coefficients $\boldsymbol{\beta}_j$, w , σ_j^2 , ρ_{jl} and τ . The posterior distribution of the latent indicator variable $\boldsymbol{\gamma} = \text{vec}\{\boldsymbol{\Gamma}\}$ can be estimated by a Metropolis-Hastings sampler.

Inference for the SUR model with hyper-inverse Wishart and MRF priors is similar to (10),

but each cumulative product in (10) with respect to the response index j or l will become a cumulative product with respect to cliques of the graph \mathcal{G} and then a cumulative product with respect to the response index of each clique. If there are random effects for sample groups as in (9), the joint posterior distribution (10) will include parameters \mathbf{B}_0 and w_0 , i.e.,

$$\begin{aligned} & f(\mathbf{B}_0, \mathbf{B}, \mathbf{\Gamma}, w_0, w, \boldsymbol{\rho}, \boldsymbol{\sigma}^2, \tau | \mathbf{Y}, \mathbf{X}, \mathbf{Z}) \\ &= f(\mathbf{Y} | \mathbf{X}, \mathbf{Z}, \mathbf{B}_0, \mathbf{B}, \boldsymbol{\rho}, \boldsymbol{\sigma}^2) f(\mathbf{B}_0 | w_0) f(w_0) f(\mathbf{B} | \mathbf{\Gamma}, w) f(\mathbf{\Gamma} | G, d, e) f(w) f(\boldsymbol{\rho} | \boldsymbol{\sigma}^2, \tau) f(\boldsymbol{\sigma}^2 | \tau) f(\tau) \end{aligned}$$

We implement Gibbs samplers to obtain posterior estimates for \mathbf{B} , $\boldsymbol{\rho}$ and $\boldsymbol{\sigma}^2$, and update the latent indicator variable $\mathbf{\Gamma}$ via a Metropolis-Hastings sampler with parallel tempering in the same way as Bottolo et al. (2021). Thompson sampling (Russo et al., 2018) is used to derive the proposal for each latent indicator γ_{kj} . The hyper-parameter τ is updated via a random walk Metropolis sampler as proposed by Bottolo et al. (2021).

To overcome the prohibitive computational time in high-dimensional settings, the ESS algorithm (Bottolo and Richardson, 2010; Richardson et al., 2011) is used to update the posteriors. For each iteration of the MCMC sampler, after sampling the latent indicator variables $\mathbf{\Gamma}$, we first update most other hyper-parameters, and then update the parameters $\boldsymbol{\sigma}^2$ and $\boldsymbol{\rho}$, and finally update the regression coefficient matrices \mathbf{B} and \mathbf{B}_0 .

1. sampling latent indicator variables $\mathbf{\Gamma}$ using the Metropolis-Hastings sampler;
2. sampling hyper-parameter τ using a random walk Metropolis sampler;
3. sampling hyper-parameter w (and w_0) using Gibbs sampling;
4. sampling the graph \mathcal{G} from the junction tree sampler (essentially Metropolis-Hastings sampling (Green and Thomas, 2013), see Bottolo et al. (2021) for more details);
5. sampling $\boldsymbol{\sigma}^2$ and $\boldsymbol{\rho}$ from the full conditional distributions (which would be the Gibbs sampler);
6. sampling coefficients \mathbf{B} (and \mathbf{B}_0) from the full conditional distributions (which would be the Gibbs sampler).

At each iteration, the ESS algorithm implements a local move to add/delete and swap the latent indicator variables within each chain, and then a global move to exchange and crossover the latent indicator variables between any two parallel tempered chains. The temperature across

all response variables is adapted based on the acceptance rate of the global exchange operator. The ESS algorithm with parallel tempering is potentially effective to search a high-dimensional model space with multiple modes (Bottolo and Richardson, 2010).

2.5 Model performance evaluation

To evaluate the performance of the proposed approach, we focus on structure recovery and prediction performance. The structure recovery includes the estimation of the latent indicator variable $\mathbf{\Gamma}$ which captures the relationships between response variables and high-dimensional predictors, and the estimation of the graph \mathcal{G} which addresses the residual relationships between response variables. Predictive accuracy of Bayesian models for new data points can be measured by the expected log pointwise predictive density (elpd), which can be assessed by leave-one-out cross-validation (LOO) or by the widely applicable information criterion (WAIC) (Vehtari et al., 2017). We also calculate the root mean squared prediction error (RMSPE) measured on an independent test data set for the median probability model (MPM) (Barbieri and Berger, 2004) in addition to the training data root mean squared error (RMSE).

Vehtari et al. (2017) proposed an efficient computation for the Bayesian LOO estimate of out-of-sample predictive fit

$$\text{elpd}_{\text{loo}} = \sum_{j=1}^m \sum_{i=1}^n \log f(y_{ij} | \mathbf{y}_{(-i)j}),$$

where $\mathbf{y}_{(-i)j}$ is the observation vector of the j th response variable except the i th observation. The LOO is estimated by

$$\widehat{\text{elpd}}_{\text{loo}} = \sum_{j=1}^m \sum_{i=1}^n \frac{1}{\frac{1}{N} \sum_{t=1}^N \frac{1}{f(y_{ij} | \boldsymbol{\vartheta}^{(t)})}},$$

where N is the length of an MCMC chain and $\boldsymbol{\vartheta}^{(t)}$ is the MCMC samples at the t th iteration for all related parameters. The WAIC is estimated by

$$\widehat{\text{elpd}}_{\text{waic}} = \widehat{\text{elpd}}_{\text{loo}} - \sum_{j=1}^m \sum_{i=1}^n \text{Var}_{t=1}^N [\log f(y_{ij} | \boldsymbol{\vartheta}^{(t)})],$$

where the second term above is used as a measure of the model complexity.

For future prediction, a single model may be required in some cases, for practical reasons or for simplicity. Barbieri and Berger (2004) suggested the median probability model (MPM),

which is defined for each coefficient to be $\mathbb{E}[\beta_{kj}|\gamma_{kj} = 1, data]$ if $\mathbb{P}\{\gamma_{kj} = 1|data\} > 0.5$, or 0 otherwise. It can be estimated through MCMC estimates:

$$\hat{\beta}_{kj,MPM} = \begin{cases} \frac{\sum_{t=1}^N \beta_{kj}^{(t)}}{\sum_{t=1}^N \gamma_{kj}^{(t)}}, & \text{if } \frac{\sum_{t=1}^N \gamma_{kj}^{(t)}}{N} > 0.5, \\ 0, & \text{otherwise,} \end{cases}$$

where $\gamma_{kj}^{(t)}$ is the estimate of the t th MCMC iteration for the latent indicator variable of β_{kj} . After obtaining $\hat{\mathbf{B}}_{MPM} = \{\hat{\beta}_{kj,MPM}\}$, the RMSE and RMSPE are

$$\begin{aligned} \text{RMSE} &= \frac{1}{\sqrt{mn}} \|\mathbf{Y} - \mathbf{X}\hat{\mathbf{B}}_{MPM}\|_2, \\ \text{RMSPE} &= \frac{1}{\sqrt{mn'}} \|\mathbf{Y}^* - \mathbf{X}^*\hat{\mathbf{B}}_{MPM}\|_2, \end{aligned}$$

where $\mathbf{Y}_{n \times m}$ and $\mathbf{X}_{n \times p}$ were used to estimate $\hat{\mathbf{B}}_{MPM}$, and $\mathbf{Y}_{n' \times m}^*$ and $\mathbf{X}_{n' \times p}^*$ are new data.

3 Simulation study

In this section, our SSUR model with MRF prior, denoted as SSUR-MRF, is evaluated with respect to structure recovery for the regression coefficient matrix and prediction performance of responses. We set up two simulation scenarios: one with independent samples and the other with heterogeneous and correlated samples. In the first scenario, our approach is compared with the SSUR model with a hotspot prior, denoted as SSUR-hotspot, which was studied by Bottolo et al. (2021). In the second scenario, our approach is compared with the SSUR-MRF model without random effects.

3.1 Simulation scenarios

We design a network shown in Figure 2(a) to construct a complex structure between 20 response variables and 300 predictors. It assumes that the 20 response variables are divided into three groups, and the first 120 predictors are divided into six groups. The first group of responses (i.e., $\{\mathbf{y}_1, \dots, \mathbf{y}_5\}$) is related to four groups of predictors (i.e., $\{\mathbf{x}_1, \dots, \mathbf{x}_5\}$, $\{\mathbf{x}_{30}, \dots, \mathbf{x}_{50}\}$, $\{\mathbf{x}_{51}, \dots, \mathbf{x}_{60}\}$ and $\{\mathbf{x}_{110}, \dots, \mathbf{x}_{120}\}$). The second group of responses (i.e., $\{\mathbf{y}_6, \dots, \mathbf{y}_{12}\}$) is also related to four predictor groups (i.e., $\{\mathbf{x}_{10}, \dots, \mathbf{x}_{20}\}$, $\{\mathbf{x}_{51}, \dots, \mathbf{x}_{60}\}$, $\{\mathbf{x}_{70}, \dots, \mathbf{x}_{90}\}$ and $\{\mathbf{x}_{110}, \dots, \mathbf{x}_{120}\}$). The third group of responses (i.e., $\{\mathbf{y}_{13}, \dots, \mathbf{y}_{20}\}$) is related to three predictor groups (i.e., $\{\mathbf{x}_{30}, \dots, \mathbf{x}_{50}\}$, $\{\mathbf{x}_{70}, \dots, \mathbf{x}_{90}\}$ and $\{\mathbf{x}_{110}, \dots, \mathbf{x}_{120}\}$). Corresponding to this

network structure between the responses and predictors, a sparse latent indicator variable $\mathbf{\Gamma}$ (Figure 2(b)) reflects the associations between the response variables and predictors in the SUR model (1). In addition, we design a decomposable graph \mathcal{G} (Figure 2(c)) to reflect the residual structure between the response variables. The graph \mathcal{G} has six blocks representing six subgroups of response variables that cannot be explained by the linear predictor \mathbf{XB} , which can make our modelling more challenging. The information \mathcal{G} is included in the residuals and can be expected to be recovered by statistical models.

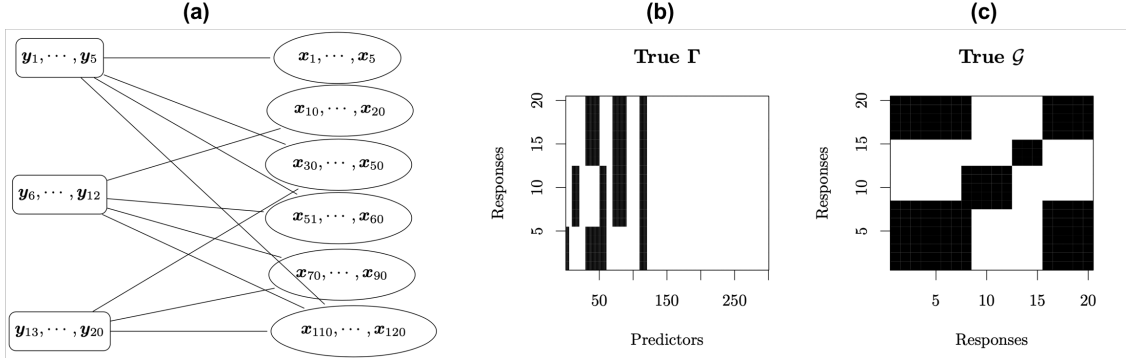


Figure 2: Simulation scenarios: True relationships between response variables and predictors. (a) Network structure between \mathbf{Y} and \mathbf{X} ; (b) latent indicator variable $\mathbf{\Gamma}$ for the associations between \mathbf{Y} and \mathbf{X} in the SUR model; (c) additional structure \mathcal{G} between response variables not explained by \mathbf{XB} . Black indicates a true relation between the response variables and predictors.

In scenario 1, the response and predictor datasets are generated based on a multivariate linear regression model

$$\mathbf{Y} = \mathbf{1}\boldsymbol{\alpha}^\top + \mathbf{XB}_\mathbf{\Gamma} + \mathbf{U}.$$

The intercepts $\boldsymbol{\alpha} = \{\alpha_j\}$ and input data $\mathbf{X} = \{x_{ik}\}$ ($i = 1, \dots, 250; k = 1, \dots, 300; j = 1, \dots, 20$) are simulated independently from the standard normal distribution. The regression coefficients $\mathbf{B} = \{\beta_{kj}\}$ ($k = 1, \dots, 300; j = 1, \dots, 20$) are also simulated independently from the standard normal distribution but truncated by the latent indicator variable $\mathbf{\Gamma} = \{\gamma_{kj}\}$, i.e., $\mathbf{B}_\mathbf{\Gamma} = \{\beta_{kj}\mathbb{1}_{\gamma_{kj}=1}\}$. The noise matrix \mathbf{U} is simulated based on the standard multivariate normal distribution $\tilde{\mathbf{U}} = \{\tilde{u}_{ij}\} \stackrel{iid}{\sim} \mathcal{N}(0, 1)$ and a G-Wishart distribution $\mathcal{W}_G(\cdot, \cdot)$ (Mohammadi and Wit, 2019). We simulate the G-Wishart distribution $P \sim \mathcal{W}_G(3, M)$ where diagonals of M are 1 and off-diagonals are 0.5, and Use Cholesky decomposition $\text{chol}(P^{-1})$ to get $\mathbf{U} = \tilde{\mathbf{U}} \cdot \text{chol}(P^{-1})$. We control the average signal-to-noise ratio defined by Bottolo et al. (2021), and set it to 10. Independent data sets \mathbf{X}^* and \mathbf{Y}^* are simulated based on the same scenario as validation data.

In scenario 2, \mathbf{X} , $\mathbf{\Gamma}$, $\mathbf{B}_\mathbf{\Gamma}$ and \mathbf{U} are generated in the same manner as scenario 1. We also

include group indicators \mathbf{Z} with independent row vectors $\mathbf{z}_i \sim \text{multinomial}(0.1, 0.2, 0.3, 0.4)$ ($i = 1, \dots, n$ and the number of groups is set to $T = 4$), and random effects $\mathbf{B}_0 = \{\beta_{0,t,j}\} \stackrel{iid}{\sim} \mathcal{N}(0, 2^2)$. The response dataset is generated from a linear mixed model

$$\mathbf{Y} = \mathbf{X}\mathbf{B}_\Gamma + \mathbf{Z}\mathbf{B}_0 + \mathbf{U}.$$

Independent validation data sets are also simulated based on scenario 2. The algorithms for the two simulation scenarios can be found in Supplementary S2.

We run a MCMC sampler with 5 chains, 400 000 iterations in total with the first 200 000 iterations as a burn-in period. Both simulation algorithms generate validation datasets independently with the same sample size to evaluate the performance of the proposed methods.

3.2 Comparison of the SSUR-hotspot and SSUR-MRF models

We first compare our proposed SSUR-MRF model to the SSUR-hotspot model on simulated data generated with scenario 1. Our approach uses the network in Figure 2(a) as prior information to construct edge potentials for the MRF prior as illustrated in Section 2.2. Throughout this article, we refer to a predictor as being selected or identified, if the corresponding latent indicator variable has posterior mean larger than 0.5. Figure 3 shows that SSUR-hotspot and our SSUR-MRF both have good recovery for the residual structure between response variables (i.e., \mathcal{G}). However, SSUR-MRF has better structure recovery of the latent indicator variable Γ . Table 1 reports higher accuracy, sensitivity and specificity of the estimator for Γ by SSUR-MRF than SSUR-hotspot. The two methods have similar $\widehat{\text{elpd}}_{\text{loo}}$ and $\widehat{\text{elpd}}_{\text{waic}}$, but our approach has smaller RMSE and RMSPE.

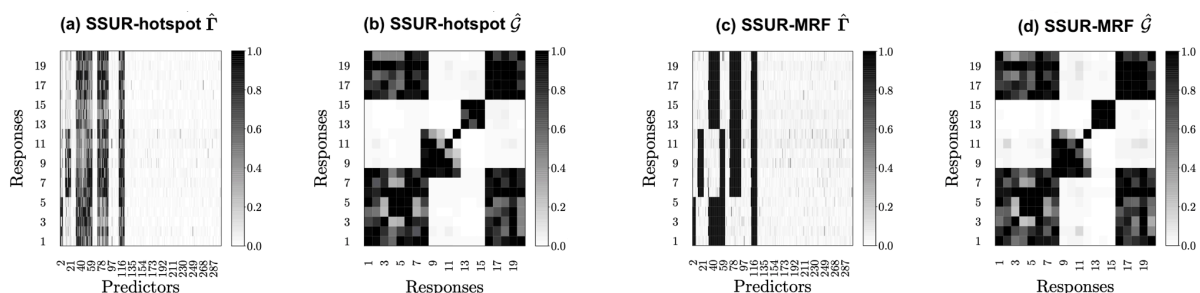


Figure 3: Results for simulation scenario 1: Posterior mean of Γ and \mathcal{G} by models SSUR-hotspot (panels (a) and (b)) and SSUR-MRF (panels (c) and (d))

Table 1: Results for simulation scenario 1: Accuracy of variable selection and prediction performance of models SSUR-hotspot and SSUR-MRF prior

	accuracy	sensitivity	specificity	$\widehat{\text{elpd}}_{\text{loo}}$	$\widehat{\text{elpd}}_{\text{waic}}$	RMSE	RMSPE
SSUR-hotspot	0.931	0.753	0.968	-21045.2	-21045.7	14.135	7.971
SSUR-MRF	0.982	0.971	0.984	-21044.6	-21045.3	13.860	7.167

3.3 Sensitivity analysis for SSUR-MRF

The MRF prior used in our approach might be strongly informative as the edge potentials were constructed according to the true relationships between the simulated response variables and predictors. Here we use different edge potentials G in the MRF prior for a sensitivity analysis. Starting from the previously constructed edge potentials G , we partially delete true edge potentials either uniformly or non-uniformly or add noise edge potentials. The three cases are as follows:

- Case 1: delete 1%, 10%, 50% or 90% edges uniformly from the fully informative G . This case always keeps some of the true associations across all patterns of $\mathbf{\Gamma}$.
- Case 2: delete 1%, 10%, 50%, 90% or 100% edges non-uniformly in consecutive chunks from the edge list* corresponding to the fully informative G . This case might remove all information about some of the associations between groups of predictors and response variables completely $\mathbf{\Gamma}$.
- Case 3: add 0.1%, 0.5%, 1%[†] noise edges to the fully informative G .

Table 2 shows that our SSUR-MRF model can identify truly associated predictors well with respect to accuracy, sensitivity and specificity of the estimated $\mathbf{\Gamma}$, and have stable prediction performance with respect to RMSE and RMSPE, when deleting 1%, 10%, 50% and 90% true edges uniformly. This indicates that our approach can recover a good structure of $\mathbf{\Gamma}$ and good prediction performance of responses, even if only a little true association knowledge across all patterns of $\mathbf{\Gamma}$ is used in the MRF prior.

When some of the patterns in $\mathbf{\Gamma}$ are fully unknown (i.e., when blocks of edges are deleted) in the MRF prior, the performance of variable selection becomes worse with respect to accuracy,

*The coordinates of all nonzero values of G are put in an edge list in order. Deleting edge potentials uniformly, for example deleting 1%, means that the $1 + (1 - 1/|\mathcal{E}|)/1\% \cdot \{0 : (1\% \cdot |\mathcal{E}|)\}$ th edges of the whole true edge list are deleted. Deleting 1% blocks of edges means that the last 1% blocks of edges are deleted. The true edge list includes the edges of each pattern (i.e., association block) together. Adding 1% noise edges means that $1\% \cdot mp(mp - 1)/2$ wrong edges are included randomly.

[†]Note that 1% noise edges are already more than the total number of true edges, which are only $\sim 0.3\%$ of all possible edges.

sensitivity and specificity. So does the prediction performance with respect to RMSPE. Figure 4 indicates that the information of the deleted blocks cannot be recovered fully, but will instead be estimated with a sparser Γ . Supplementary S3 shows slightly worse residual structure recovery (i.e., $\hat{\mathcal{G}}$) when deleting more block edges. Table 2 shows stable variable selection and prediction performance when adding noise edges in the MRF prior. Here, $\widehat{\text{elpd}}_{\text{loo}}$ and $\widehat{\text{elpd}}_{\text{waic}}$ do not change much between different cases, but they can be used as the objective function to optimize some hyperparameters.

Table 2: Results for simulation scenario 1: Sensitivity analysis of SSUR-MRF with different MRF priors

	accuracy	sensitivity	specificity	$\widehat{\text{elpd}}_{\text{loo}}$	$\widehat{\text{elpd}}_{\text{waic}}$	RMSE	RMSPE
Case 1							
delete edges uniformly							
1%	0.981	0.969	0.983	-21049.5	-21049.8	13.843	7.191
10%	0.981	0.969	0.984	-21044.4	-21045.0	13.847	7.157
50%	0.982	0.970	0.984	-21044.7	-21045.4	13.849	7.173
90% [†]	0.980	0.955	0.986	-21044.3	-21045.1	13.846	7.283
Case 2							
delete edges non-uniformly							
1%	0.982	0.971	0.984	-21044.9	-21045.6	13.853	7.174
10%	0.976	0.928	0.985	-21044.7	-21045.3	13.817	7.231
50%	0.945	0.734	0.989	-21044.6	-21045.3	14.279	8.026
90% [†]	0.921	0.623	0.982	-21044.8	-21045.5	14.367	8.054
100% [†]	0.900	0.570	0.968	-21035.0	-21035.2	14.351	8.222
Case 3							
add noise edges							
0.1%	0.982	0.969	0.985	-21045.1	-21045.7	13.847	7.161
0.5%	0.982	0.969	0.984	-21044.9	-21045.6	13.858	7.171
1%	0.982	0.970	0.984	-21044.5	-21045.2	13.851	7.158

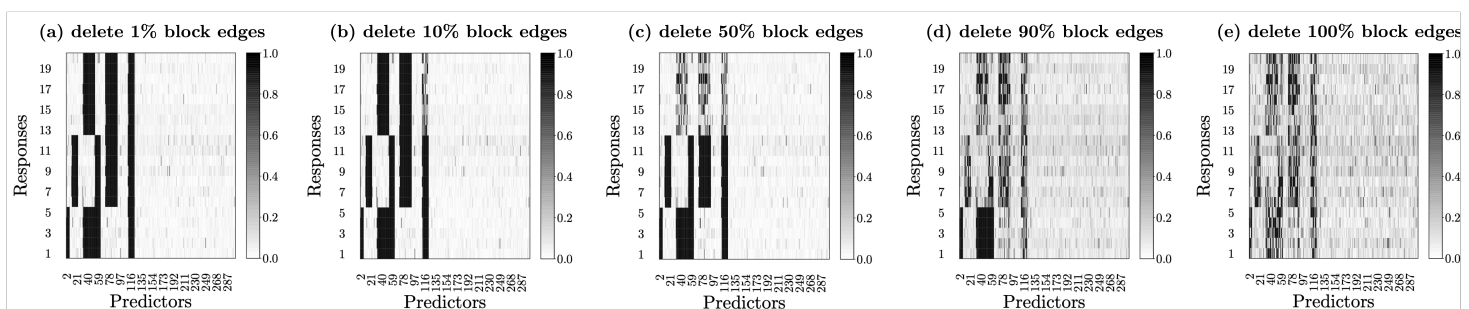


Figure 4: Results for simulation scenario 1: Sensitivity analysis for case 2, i.e. when blocks of edges are deleted.

3.4 Results and discussion of SSUR-MRF with random effects

In the simulation scenario 2, $T = 4$ sample group variables are simulated to assess the performance of our SSUR-MRF model with random effects. As described in Section 2.1 and 2.3, the hyper-parameters of random effects and shrinkage coefficients need to be specified appropriately for the model without data standardization. We assume $\mathbb{E}[\beta_{0,kj}] = 0$ and $\mathbb{V}\text{ar}[\beta_{0,kj}] = 2^2$. Since $\mathbb{E}[\beta_{0,kj}] + 1.96\sqrt{\mathbb{V}\text{ar}[\beta_{0,kj}]} = 3.92$ and $r_{sparsity} = 1$, we choose $const_{a_{w_0}} = 1/30$ and $b_{w_0} = 500$ so that

$$a_{w_0} = const_{a_{w_0}} \cdot 1/2 \cdot m \cdot p \cdot r_{sparsity} = 100,$$

and the 5% quantile of $\mathcal{IG}(a_{w_0}, b_{w_0})$ is $4.27 > 3.92$. Similarly but assuming $r_{sparsity} = 0.1$, $\mathbb{E}[\beta_{kj}] = -0.1$, $\mathbb{V}\text{ar}[\beta_{kj}] = 1$, $const_{a_w} = 1/20$ and $const_{b_w} = 20$ for shrinkage coefficients, we obtain $a_w = 15$ and $b_w = 60$. For the hyperparameters d and e in a MRF prior, we assume the model sparsity in the range $(c_1, c_2) = (0.1, 0.2)$, and then $d = \text{logit } c_1 = -2$ and grid interval $e = (0, -d - \ln(c_2^{-1} - 1)) = (0, 0.6]$.

Figure 5(a), 5(c) and Table 3 show similar recovery of the latent indicator variable Γ with respect to accuracy, sensitivity and specificity for both SSUR-MRF with and without random effects. However, $\frac{1}{\sqrt{mp}} \|\hat{\mathbf{B}}_{MPM} - \mathbf{B}\|_{\ell_2}^2$ by SSUR-MRF without random effects has slightly larger error (0.268) of SSUR-MRF with random effects (0.255). In addition, the SSUR-MRF model without random effects has difficulty recovering the residual graph structure \mathcal{G} (Figure 5(d)), while the model with random effects can identify the true structure without problems (Figure 5(b)). See also Table 3, which reports the recovery performance of \mathcal{G} with respect to accuracy, sensitivity and specificity when thresholding at 0.5. For the response prediction, SSUR-MRF with random effects has smaller $\widehat{\text{elpd}}_{\text{loo}}$, $\widehat{\text{elpd}}_{\text{waic}}$ and RMSE but slightly larger RMSPE than SSUR-MRF without random effects (Table 3).

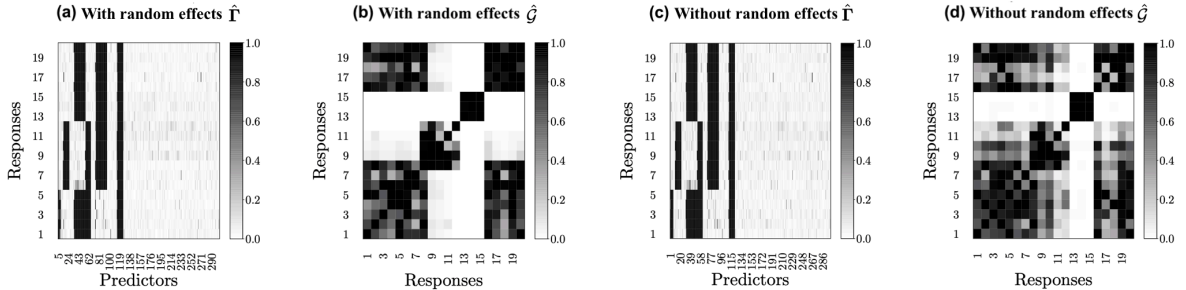


Figure 5: Results for simulation scenario 2: Posterior mean of Γ and \mathcal{G} by the SSUR-MRF with random effects based on the simulated data from scenario 2

Table 3: Results for simulation scenario 2: Structure recovery and prediction by SSUR-MRF with and without random effects

	accuracy	sensitivity	specificity	$\widehat{\text{elpd}}_{\text{loo}}$	$\widehat{\text{elpd}}_{\text{waic}}$	RMSE	RMSPE
With random effects				-21138.0	-21138.8	14.248	7.148
Γ	0.980	0.960	0.984				
\mathcal{G}	0.895	0.792	1.000				
Without random effects				-21148.5	-21149.1	14.435	7.040
Γ	0.980	0.962	0.984				
\mathcal{G}	0.755	0.683	0.828				

4 Application to a pharmacogenomic screen

We apply our approach to a subset of the Genomics of Drug Sensitivity in Cancer (GDSC) database (Yang et al., 2013; Garnett et al., 2012) to study the relationships between multiple cancer drugs and high-dimensional genomic features characterising cancer cell lines. The pharmacological and genomic data are from <ftp://ftp.sanger.ac.uk/pub4/cancerrxgene/releases/release-5.0/> preprocessed by Garnett et al. (2012). We would like to investigate how the MRF prior can help to improve inference for groups of drugs that are known to have correlated response; we therefore select two groups of cancer drugs with similar molecular targets and the generic non-targeted chemotherapy agent Methotrexate:

- four MAPK inhibitors, i.e., RDEA119, PD-0325901, CI-1040 and AZD6244,
- two Bcr-Abl tyrosine kinase inhibitors, i.e., Nilotinib and Axitinib,
- and one generic chemotherapy agent, Methotrexate.

The seven drugs were tested on 499 cell lines from 13 cancer tissue types with complete drug sensitivity values. The drug sensitivity of the cell lines was summarized by the $\log_{10}(\text{IC}_{50})$ from *in vitro* drug concentration response experiments. Note that smaller $\log_{10}(\text{IC}_{50})$ values indicate higher sensitivity of a cell line to the drug; therefore a negative regression coefficient indicates that a positive increment of the value of a feature is associated with an increase in drug sensitivity. In order to explore the relationships between the three groups of drugs and the genomic profiles of the cell lines, we first preselect known cancer genes and their corresponding genomic features by following Garnett et al. (2012), including 426 copy number variation features (counts) and 68 mutated features (binary). To make a trade-off between the computational efficiency and amount of information from gene expression data, we then preselect three subsets

of gene expression features with the largest variances over cell lines, which explain 10%, 30% and 50% of the variation, which results in 269, 1175 and 2602 gene expression features, respectively. This creates three data sets including both gene expression, copy number variation and mutation information, to predict drug sensitivity responses, i.e.,

- Feature set I with 763 predictors,
- Feature set II with 1669 predictors,
- Feature set III with 3096 predictors.

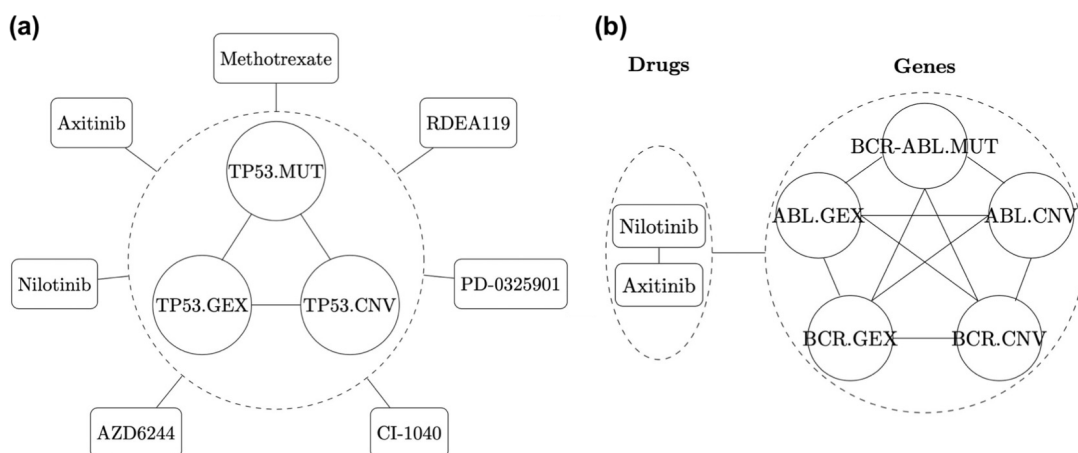


Figure 6: GDSC data application: Illustration of the assumed relationships between drugs and related gene features, which are used for the MRF prior. The right panel is for the Bcr-Abl fusion gene, its corresponding related features and the two Bcr-Abl tyrosine kinase inhibitor drugs. The left panel illustrates gene TP35 as one example with its corresponding features representing all three data sources; all seven drugs are shown to indicate that the relationship between the three gene features is valid in relation to all drugs in the data set. The rectangles indicate drugs, solid circles indicate gene features and dashed circles indicate that the elements inside are related. The edges between drugs and dashed circled gene features indicate assumed associations between the gene features and the drug sensitivity measurements for the drugs. The names with suffix “.GEX”, “.CNV” and “.MUT” indicate features of expression, copy number variation and mutation, respectively.

To construct edge potentials for the MRF prior in the proposed model (9) in Section 2.3, we summarize some known biological relationships between the drugs and genomic information. First, all features (gene expression, copy number variation, mutation) corresponding to the same gene are assumed to be related. This group of features are likely to be identified together corresponding to each drug, i.e., if one feature for a certain gene is a predictor of drug sensitivity, then the other features corresponding to the same gene are more likely to be predictors as well.

The illustration of Figure 6(a)) constructs edge potentials

$$\underbrace{G_y}_{7 \text{ drugs}} \otimes \underbrace{G_x}_{3 \text{ features}} - \mathbb{I}_{21} = \mathbb{I}_7 \otimes \begin{pmatrix} 1 & 1 & 1 \\ 1 & 1 & 1 \\ 1 & 1 & 1 \end{pmatrix} - \mathbb{I}_{21}.$$

Second, the two Bcr-Abl tyrosine kinase inhibitors were developed to inhibit Bcr-Abl tyrosine kinase activity and proliferation of Bcr-Abl expressing cells, so the point mutation BCR-ABL, and features associated with genes BCR and ABL are related and likely to be identified together corresponding to the two Bcr-Abl inhibitors. The illustration of Figure 6(b)) constructs edge potentials

$$\underbrace{G_y}_{2 \text{ drugs}} \otimes \underbrace{G_x}_{5 \text{ features}} - \mathbb{I}_{10} = \begin{pmatrix} 1 & 1 \\ 1 & 1 \end{pmatrix} \otimes \begin{pmatrix} 1 & 1 & 1 & 1 & 1 \\ 1 & 1 & 1 & 1 & 1 \\ 1 & 1 & 1 & 1 & 1 \\ 1 & 1 & 1 & 1 & 1 \\ 1 & 1 & 1 & 1 & 1 \end{pmatrix} - \mathbb{I}_{10}.$$

Third, the four MAPK inhibitors were developed to reduce the activity of the MAPK pathway, so the genes representing the MAPK pathway are considered related and likely to be identified together as potential predictor variables for drug sensitivity of the four MAPK inhibitors. Based on the set of genes linked to the MAPK pathway from the Kyoto Encyclopedia of Genes and Genomes (KEGG) PATHWAY database, we can construct edge potentials for the MRF prior with respect to the three feature sets, respectively. Here an element of the G matrix can be 2 representing an edge weight of 2, if the corresponding two features are both from the same gene and also belong to one group of target genes.

To specify weak informative priors for the random effects for the 13 cancer tissue types, we assume that the effect of each cancer tissue has prior mean 0 and prior standard deviation 3, which results in the hyper-parameters $w_0 \sim \mathcal{IG}(54.6, 400)$ according to the prior specification in Section 2.3. Corresponding to the three feature sets, the model sparsity is assumed to be 6%, 2% and 1% respectively [‡], so we obtain parameter d in the MRF prior with values -2.7, -4 and -4.6. Our SSUR-MRF model with random effects, hereafter denoted as SSUR-MRF, has good MCMC diagnostics (see Supplementary S5). For comparison, we run a similar model with parameter $e = 0$ in the MRF prior, which is equivalent to independent Bernoulli priors for the indicator variables, here denoted as SSUR-Ber. In SSUR-Ber, the model sparsity hyper-parameter d in the prior $f(\gamma|d) \propto \exp\{d\mathbb{1}^\top \gamma\}$ is tuned to reach the best elpd_{loo} and $\text{elpd}_{\text{waic}}$.

Figure 7 shows an estimated residual structure between the seven drugs by our SSUR-MRF

[‡]We assume there are roughly 50 associated features for each response variables based on the number of target genes. Then the assumed model sparsity is 50 divided by the total number of features, i.e., 50/763, 50/1699 and 50/3096.

model based on Feature set III. It does not only estimate residual correlation between any two MAPK inhibitors and between the two Bcr-Abl inhibitors, but also separates the chemotherapy drug Methotrexate from the other drugs. Supplementary S6 shows the residual structures between the seven drugs as estimated by the SSUR-MRF and SSUR-Ber models with feature sets I-III, respectively. We find that the structure estimated by our SSUR-MRF model based on feature set III is closest to our knowledge about the relationships between the seven drugs.

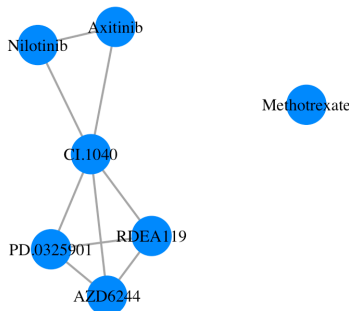


Figure 7: GDSC data application: Estimated residual structure between the seven drugs by the SSUR-MRF model based on features set III with \hat{G} thresholded at 0.5.

Table 4: GDSC data application: Number of identified genomic features corresponding to each drug by the SSUR-Ber and SSUR-MRF models.

	Nilotinib	Axitinib	RDEA119	PD-0325901	CI-1040	AZD6244	Methotrexate
SSUR-Ber							
Feature set I	5	5	2	3	1	0	3
Feature set II	1	2	3	1	1	2	2
Feature set III	8	11	8	4	8	10	8
SSUR-MRF							
Feature set I	1	2	42	41	40	40	0
Feature set II	9	10	56	56	56	57	9
Feature set III	39	38	87	86	86	89	41

To look at variable selection, a gene feature is identified if the estimated marginal selection probability of its coefficient is larger than 0.5, i.e., if the corresponding latent indicator variable has posterior mean larger than 0.5. Table 4 reports the numbers of identified features over the seven drugs by the SSUR-Ber and SSUR-MRF models. SSUR-Ber results in very sparse models and identifies a similar number of genomic features for each drug. In contrast, our SSUR-MRF model identifies more genomic features and finds a different model sparsity for the three drug groups, in particular relatively denser models for the four MAPK inhibitors. This indicates that our model is able to distinguish variable selection corresponding to different response variables.

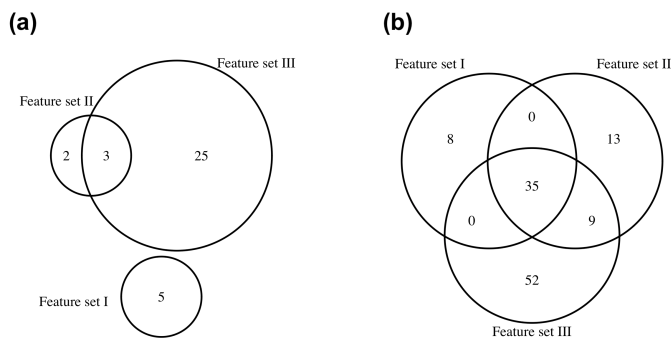


Figure 8: GDSC data application: A Venn diagram for the numbers of identified features for the MAPK inhibitors by SSUR-Ber (panel (a)) and SSUR-MRF (panel (b)) models and overlaps between the models fitted with feature sets I, II, and III.

For the group with the two BCR-ABL inhibitors, i.e., Nilotinib and Axitinib, both SSUR-Ber and SSUR-MRF identify the mutation BCR-ABL associated to drug Nilotinib, as expected. For the group of the four MAPK inhibitors, Figure 8 displays the numbers of any identified features for the MAPK inhibitors by SSUR-Ber and SSUR-MRF. For feature sets I, II and III, SSUR-Ber identifies quite different features (Figure 8(a)), i.e. there is not much overlap. However, our SSUR-MRF model identifies 35 common features over the three feature sets. This reflects more stable variable selection that is achieved by using prior knowledge via the MRF prior. Table 5 further shows that the SSUR-Ber model with independent Bernoulli priors does not identify any known target features for the MAPK inhibitors. Supplementary Table S7.1 shows the identified feature names for the MAPK inhibitors by SSUR-Ber. Nevertheless, our SSUR-MRF model is able to identify many more features than SSUR-Ber, and identifies more known target features for the MAPK inhibitors. Figure 9 shows the names of the identified features for the MAPK inhibitors by SSUR-MRF. The seven copy number variation and mutation features in Figure 9(a) are also in Figure 9(b) and (c). This is because only more gene expression features are selected by the models using feature sets II and III, but no additional mutations or CNV features. As more target gene expression features are used to construct the edge potentials in the MRF prior in the models built with feature sets II and III, our approach can identify more of them.

As Figure 8(b) shows, we have identified 35 common features with the SSUR-MRF model over feature sets I, II and III, but only seven of these common features belong to known target genes of the corresponding drugs as shown in Figure 9. We have found that 28 other common identified features are cancer genes, i.e. genes that are known to be deregulated in cancer. They are listed in Supplementary Table S7.2. The Cancer Gene Census has reported how dysfunction of these genes drives cancer (Sondka et al., 2018).

Table 5: GDSC data application: Numbers of genomic features selected as predictors for the MAPK inhibitors in the SSUR-Ber and SSUR-MRF models. Note that Feature sets I, II and III include 40, 55, and 81 features corresponding to known target genes of the corresponding drug, respectively.

	SSUR-Ber (%)	SSUR-MRF (%)
Feature set I		
$\frac{\# \text{ identified targets}}{\# \text{ known targets}}$	0/40 (0%)	7/40 (17.5%)
$\frac{\# \text{ identified targets}}{\# \text{ identified features}}$	0/5 (0%)	7/43 (16.3%)
Feature set II		
$\frac{\# \text{ identified targets}}{\# \text{ known targets}}$	0/55 (0%)	8/55 (14.5%)
$\frac{\# \text{ identified targets}}{\# \text{ identified features}}$	0/5 (0%)	8/57 (14.0%)
Feature set III		
$\frac{\# \text{ identified targets}}{\# \text{ known targets}}$	0/81 (0%)	17/81 (21.0%)
$\frac{\# \text{ identified targets}}{\# \text{ identified features}}$	0/28 (0%)	17/96 (17.7%)

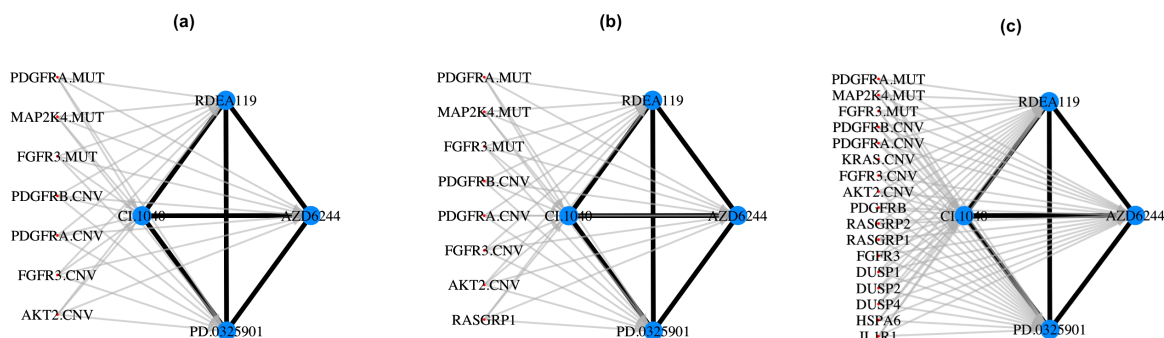


Figure 9: GDSC data application: Estimated network between the MAPK inhibitors and identified target genes based on \hat{G} and $\hat{\Gamma}$ thresholded at 0.5 by SSUR-MRF corresponding to feature set I, II and III respectively.

In Table 6, prediction performances of the SSUR-Ber and SSUR-MRF models are reported based on Feature set III which has the most genomic information. With respect to elpd.LOO or elpd.WAIC, our SSUR-MRF model is slightly worse than SSUR-Ber. For out-sample prediction, we need an independent data set to calculate RMSPE. Smirnov et al. (2016) provides an updated GDSC data set, in which we gathered 46 different cell lines with complete pharmacogenomic data. Table 6 shows that our SSUR-MRF model has slightly better RMSPE than SSUR-Ber.

Table 6: GDSC data application: Prediction performance of the SSUR-Ber and SSUR-MRF models based on Feature set III.

	SSUR-Ber	SSUR-MRF
elpd.LOO	-8136	-8143
elpd.WAIC	-8169	-8178
RMSE	2.003	1.883
RMSPE	2.095	2.062

Our approach also estimates the effects of 13 cancer tissue types, which may indicate certain relationship between drugs and cancer types. Figure 10 shows the estimated random effects by SSUR-MRF using the genomic feature set III. Negative effect estimates can indicate specific effectiveness of drugs to kill cancer cells of the corresponding cancer type. We focus on strong (negative) effects, since most error bars (i.e., standard deviations) of the posterior mean for the cancer tissue random effects are quite large. Methotrexate has the strongest average effect in blood cancer samples; it is known to be an effective chemotherapeutic agent in leukemia (Powell et al., 2010). Supplementary S8 shows that Methotrexate has much lower $\log(\text{IC}_{50})$ values on cell lines from blood tissue type compared with other tissue types. PD-0325901 has the strongest effect in skin cancer samples. Supplementary S9 also shows that PD-0325901 has much lower $\log(\text{IC}_{50})$ values on cell lines from skin tissue type compared with other tissue types. Nilotinib and Axitinib are common targeted treatments for chronic myelogenous leukemia cases with a BCR-ABL mutation (Halbach et al., 2016). We can observe their effect on blood cancer samples in Figure 10 although with large error bars, and their quite low $\log(\text{IC}_{50})$ on the only four BCR-ABL mutated blood cancer samples in Supplementary S9.

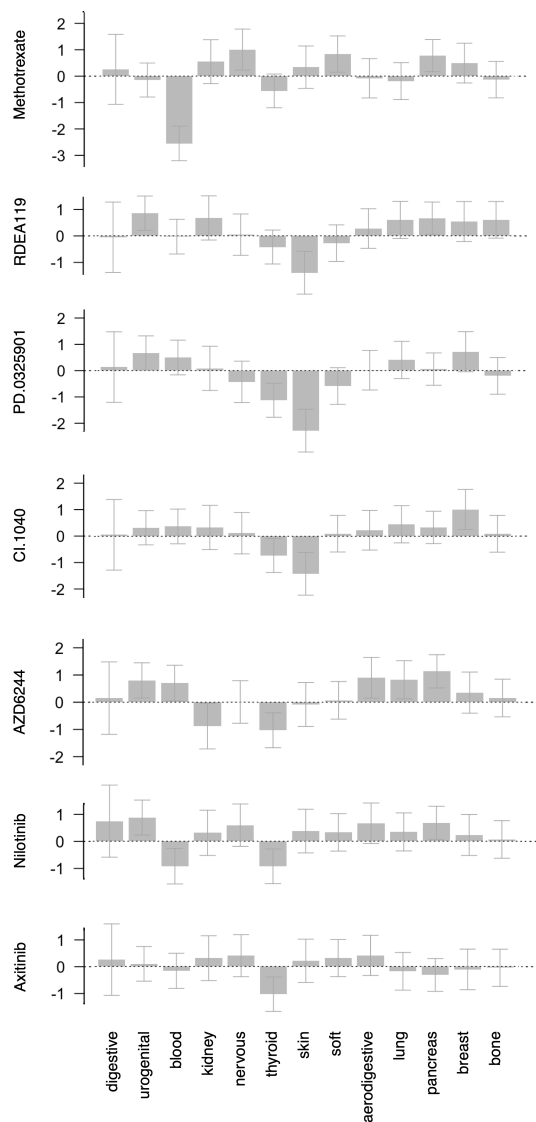


Figure 10: GDSC data application: Posterior estimates for the cancer tissue random effects for all drugs based on the median probability model. Random effects are centred around zero. Error bars are \pm standard deviation of the posterior mean.

5 Discussion

In this work, we have developed a structured multivariate Bayesian variable selection model to exploit relationships between multiple correlated response variables and high-dimensional structured predictors for variable selection, and to improve prediction as well. With our approach we want to **(a)** be able to borrow known information between response variables and predictors, **(b)** learn the network between response variables and predictors, and **(c)** understand the residual covariance of response variables. The proposed approach allows us to make use of known network

information (i.e., on the relationships between responses and predictors) in an MRF prior for the selection indicator variable Γ , and to further simultaneously select predictors in a sparse manner and learn residual covariance matrix between response variables. In addition, we can take into account sample heterogeneity through random effects which are excluded from the variable selection. Guidance for specifying (weakly) informative hyper-parameters in our approach has been provided.

Through the simulation studies, we have demonstrated that the proposed approach can recover the network structure (i.e., latent indicator variable Γ) between multiple response variables and predictors, and predict responses well. We find that even including only a small amount of prior knowledge for most patterns/network groups (Figure 4(d)) will improve model performance over a model that does not include prior knowledge. Our approach is also robust to noise in the prior information (i.e., false edge potentials) in the MRF prior (Table 2). However, without any prior association knowledge between drugs and genes/pathways (i.e. subgraphs) as Figure 1 shows, it is difficult to identify true associations through our simulations in the sensitivity analysis Case 2 in Section 3.3; only a few true associations can be estimated, but many false associations appear (Figure 4(e)).

In the real data analysis, our approach can robustly identify targeted genes for the targeted therapy drugs, and also validate other cancer related genes. The use of known information for the MRF prior can improve the prediction performance of independent pharmacogenomic data (i.e. RMSPE) compared with SSUR-Ber when applying to the most data Feature set III. Through the random effects in our approach, the cancer tissue effects are estimated, which may indicate certain relationship between drugs and cancer types. Nevertheless, there can be still heterogeneity within cancer types due to certain cancer subtypes. Alternatives can be to extend our model to multilevel random effects or employ a flexible Dirichlet process for the random effect (Li et al., 2010; Heinzl et al., 2012).

Although our approach has been studied in the simulations and the application for multiple correlated response variables and high-dimensional predictors, it might be too computationally demanding if the model is not assumed to be very sparse (i.e. number of true associated features $\ll mp$). An alternative is to change our MCMC sampling approach to approximate inference, for example, variational inference that approximates posterior densities (Blei et al., 2017; Zhang et al., 2019; Münch et al., 2021).

Supplementary Materials

Software in the form of R package **BayesSUR** is available from the Comprehensive R Archive Network (CRAN) at <https://CRAN.R-project.org/package=BayesSUR> and all R codes for the simulated studies and real data analysis are available on <https://github.com/zhizuio/BayesSUR-RE>. The attached supplementary materials include the derivation of the roughly expected hyper-parameter e in a MRF prior (Supplementary S1), algorithms for the two simulation scenarios (Supplementary S2), estimated underlying graphs of the hyper-inverse Wishart prior in Section 3.3 (Supplementary S2), sensitivity analysis for the underlying graph of the a hyper-inverse Wishart prior (Supplementary S4), and more results of the GDSC data analysis are in Supplementary S5-S9.

Acknowledgements

This work was supported by the Faculty of Medicine, University of Oslo (ZZ, MZ), the Norwegian national research school in bioinformatics, biostatistics and systems biology (ZZ), Research Council of Norway project No. 237718 “Big Insight” (ZZ), European Union Horizon 2020 grant agreements No. 847912 “RESCUER” (MZ) and No. 633595 “DynaHealth” (AL), UK Medical Research Council grants MR/M013138/1 (MB, AL). The authors thank Dr. Leonardo Bottolo for discussions.

References

- Ando, T. and Zellner, A. (2010). Hierarchical bayesian analysis of the seemingly unrelated regression and simultaneous equations models using a combination of direct monte carlo and importance sampling techniques. *Bayesian Analysis*, 5(1):65–95.
- Barbieri, M. M. and Berger, J. O. (2004). Optimal predictive model selection. *The Annals of Statistics*, 32(3):870–897.
- Barretina, J., Caponigro, G., Stransky, N., Venkatesan, K., Margolin, A., Kim, S., Wilson, C., Lehar, J., Kryukov, G., Sonkin, D., and *others* (2012). The cancer cell line encyclopedia enables predictive modelling of anticancer drug sensitivity. *Nature*, 483(7391):603–607.
- Bhadra, A. and Mallick, B. (2013). Joint high-dimensional bayesian variable and covariance selection with an application to eqtl analysis. *Biometrics*, 69(2):447–457.

- Blei, D. M., Kucukelbir, A., and McAuliffe, J. D. (2017). Variational inference: A review for statisticians. *Journal of the American Statistical Association*, 112(518):859–877.
- Bottolo, L., Banterle, M., Richardson, S., Ala-Korpela, M., Järvelin, M.-R., and Lewin, A. (2021). A computationally efficient bayesian seemingly unrelated regressions model for high-dimensional quantitative trait loci discovery. *Journal of the Royal Statistical Society: Series C (Applied Statistics)*, First published: 08 May 2021.
- Bottolo, L., Petretto, E., Blankenberg, S., Cambien, F., Cook, S. A., Tiret, L., and Richardson, S. (2011). Bayesian detection of expression quantitative trait loci hot-spots. *Genetics*, 189(4):1449–1459.
- Bottolo, L. and Richardson, S. (2010). Evolutionary stochastic search for bayesian model exploration. *Bayesian Analysis*, 5(3):583–618.
- Brown, P., Vannucci, M., and Fearn, T. (1998). Multivariate bayesian variable selection and prediction. *Journal of the Royal Statistical Society, Series B (Statistical Methodology)*, 60(3):627–641.
- Carvalho, C. M., Massam, H., and West, M. (2007). Simulation of hyper-inverse wishart distributions in graphical models. *Biometrika*, 94(3):647–659.
- Deshpande, S. K., Ročková, V., and George, E. I. (2019). Simultaneous variable and covariance selection with the multivariate spike-and-slab lasso. *Journal of Computational and Graphical Statistics*, 28(4):921–931.
- Fitch, A., Jones, M., and Massam, H. (2014). The performance of covariance selection methods that consider decomposable models only. *Bayesian Analysis*, 9(3):659–684.
- Garnett, M., Edelman, E., Heidorn, S., Greenman, C., Dastur, A., Lau, K., Greninger, P., Thompson, I., Luo, X., Soares, J., Liu, Q., and *others* (2012). Systematic identification of genomic markers of drug sensitivity in cancer cells. *Nature*, 483(7391):570–575.
- George, E. I. and McCulloch, R. E. (1993). Variable selection via gibbs sampling. *Journal of the American Statistical Association*, 88(423):881–889.
- Gray, J. W. and Mills, G. B. (2015). Large-scale drug screens support precision medicine. *Cancer Discovery*, 5(11):1130–1132.

- Green, P. J. and Thomas, A. (2013). Sampling decomposable graphs using a markov chain on junction trees. *Biometrika*, 100(1):91–110.
- Halbach, S., Hu, Z., Gretzmeier, C., Ellermann, J., Wöhrle, F., Dengjel, J., and Brummer, T. (2016). Axitinib and sorafenib are potent in tyrosine kinase inhibitor resistant chronic myeloid leukemia cells. *Cell Communication and Signaling*, 14:6.
- Heinzl, F., Fahrmeir, L., and Kneib, T. (2012). Additive mixed models with dirichlet process mixture and p-spline priors. *AStA Advances in Statistical Analysis*, 96:47–68.
- Holmes, C., Denison, D., and Mallick, B. (2002). Accounting for model uncertainty in seemingly unrelated regressions. *Journal of Computational and Graphical Statistics*, 11(3):533–551.
- Jia, Z. and Xu, S. (2007). Mapping quantitative trait loci for expression abundance. *Genetics*, 176(1):611–623.
- Kim, E., Dede, M., Lenoir, W. F., Wang, G., Srinivasan, S., Colic, M., and Hart, T. (2019). A network of human functional gene interactions from knockout fitness screens in cancer cells. *Life Science Alliance*, 2(2).
- Lee, K. H., Tadesse, M. G., Baccarelli, A. A., Schwartz, J., and Coull, B. A. (2017). Multivariate bayesian variable selection exploiting dependence structure among outcomes: Application to air pollution effects on dna methylation. *Biometrics*, 73(1):232–241.
- Lewin, A., Saadi, H., Peters, J. E., Moreno-Moral, A., Lee, J. C., Smith, K. G., Petretto, E., Bottolo, L., and Richardson, S. (2016). Mt-hess: an efficient bayesian approach for simultaneous association detection in omics datasets, with application to eqtl mapping in multiple tissues. *Bioinformatics*, 32(4):523–532.
- Li, F. and Zhang, N. R. (2010). Bayesian variable selection in structured high-dimensional covariate spaces with applications in genomics. *Journal of the American Statistical Association*, 105(491):1202–1214.
- Li, Y., Lin, X., and Müller, P. (2010). Bayesian inference in semiparametric mixed models for longitudinal data. *Biometrics*, 66(1):70–78.
- Mohammadi, R. and Wit, E. (2019). Bdgraph: An r package for bayesian structure learning in graphical models. *Journal of Statistical Software*, 89(3):1–30.

- Münch, M. M., van de Wiel, M. A., Richardson, S., and Leday, G. G. R. (2021). Drug sensitivity prediction with normal inverse gaussian shrinkage informed by external data. *Biometrical Journal*, 63(2):289–304.
- Pemovska, T., Kontro, M., Yadav, B., Edgren, H., Eldfors, S., Sz wajda, A., Almusa, H., Bespalov, M. M., Ellonen, P., Elonen, E., Gjertsen, B. T., Karjalainen, R., Kuleskiy, E., Lagström, S., Lehto, A., Lepistö, M., Lundán, T., Majumder, M. M., Marti, J. M. L., Mattila, P., Murumägi, A., Mustjoki, S., Palva, A., Parsons, A., Pirttinen, T., Rämetsä, M. E., Suvela, M., Turunen, L., Västriik, I., Wolf, M., Knowles, J., Aittokallio, T., Heckman, C. A., Porkka, K., Kallioniemi, O., and Wennerberg, K. (2013). Individualized systems medicine strategy to tailor treatments for patients with chemorefractory acute myeloid leukemia. *Cancer Discovery*, 3(12):1416–1429.
- Petretto, E., Bottolo, L., Langley, S. R., Heinig, M., Mcdermott-Roe, C., Sarwar, R., Pravenec, M., Hubner, N., Aitman, T. J., Cook, S. A., and Richardson, S. (2010). New insights into the genetic control of gene expression using a bayesian multi-tissue approach. *PLoS Computational Biology*, 6(4):e1000737.
- Powell, B. L., Moser, B., Stock, W., Gallagher, R. E., Willman, C. L., Stone, R. M., Rowe, J. M., Coutre, S., Feusner, J. H., Gregory, J., Couban, S., Appelbaum, F. R., Tallman, M. S., and Larson, R. A. (2010). Arsenic trioxide improves event-free and overall survival for adults with acute promyelocytic leukemia: North american leukemia intergroup study c9710. *Blood*, 116(19):3751–3757.
- Richardson, S., Bottolo, L., and Rosenthal, J. S. (2011). Bayesian models for sparse regression analysis of high dimensional data. *Bayesian Statistics 9*, pages 539–568.
- Ruffieux, H. (2019). Large-scale variational inference for bayesian joint regression modelling of high-dimensional genetic data. *PhD dissertation*.
- Russo, D. J., Roy, B. V., Kazerouni, A., Osband, I., and Wen, Z. (2018). A tutorial on thompson sampling. *Foundations and Trends in Machine Learning*, 11(1):1–96.
- Smirnov, P., Safikhani, Z., El-Hachem, N., Wang, D., She, A., Olsen, C., Freeman, M., Selby, H., Gendoo, D. M., Grossmann, P., Beck, A. H., Aerts, H. J., Lupien, M., Goldenberg, A., and Haibe-Kains, B. (2016). Pharmacogx: an r package for analysis of large pharmacogenomic datasets. *Bioinformatics*, 32(8):1244–1246.

- Sondka, Z., Bamford, S., Cole, C. G., Ward, S. A., Dunham, I., and Forbes, S. A. (2018). The cosmic cancer gene census: describing genetic dysfunction across all human cancers. *Nature Review Cancer*, 18:696–705.
- Stingo, F. C., Chen, Y. A., Tadesse, M. G., and Vannucci, M. (2011). Incorporating biological information into linear models: A bayesian approach to the selection of pathways and genes. *Ann. Appl. Stat.*, 5(3):1978–2002.
- Vehtari, A., Gelman, A., and Gabry, J. (2017). Practical bayesian model evaluation using leave-one-out cross-validation and waic. *Statistics and Computing*, 27(5):1413–1432.
- Wang, H. (2010). Sparse seemingly unrelated regression modelling: Applications in finance and econometrics. *Comput. Stat. Data Anal.*, 54(11):2866–2877.
- Yang, W., Soares, J., Greninger, P., Edelman, E., Lightfoot, H., Forbes, S., Bindal, N., Beare, D., Smith, J., Thompson, I., Ramaswamy, S., Futreal, P., Haber, D., Stratton, M., Benes, C., McDermott, U., and Garnett, M. (2013). Genomics of drug sensitivity in cancer (gdsc): a resource for therapeutic biomarker discovery in cancer cells. *Nucleic Acids Reserch*, 41(Database issue):D955–61.
- Zellner, A. and Ando, T. (2010). A direct monte carlo approach for bayesian analysis of the seemingly unrelated regression model. *Journal of Econometrics*, 159(1):33–45.
- Zhang, C., Butepage, J., Kjellstrom, H., and Mandt, S. (2019). Advances in variational inference. *IEEE Transactions on Pattern Analysis & Machine Intelligence*, 41(8):2008–2026.
- Zhao, Z., Banterle, M., Bottolo, L., Richardson, S., Lewin, A., and Zucknick, M. (2021). Bayessur: An r package for high-dimensional multivariate bayesian variable and covariance selection in linear regression. *Journal of Statistical Software (accepted)*, arXiv: 2104.14008.

Supplementary materials for “Structured Bayesian variable selection for multiple related response variables and high-dimensional predictors”

S1: Expected upper bound for e in the MRF prior

A MRF prior

$$f(\boldsymbol{\gamma}|d, e, G) \propto \exp\{d\mathbb{1}^\top \boldsymbol{\gamma} - e\boldsymbol{\gamma}^\top G\boldsymbol{\gamma}\}$$

corresponds to a set of conditional Bernoulli distributions given by

$$f(\gamma_j|\boldsymbol{\gamma}_{-(j)}d, e, G) = p_j^{\gamma_j}(1 - p_j)^{1-\gamma_j},$$

where

$$p_j = \frac{1}{1 + \exp(-d - e \sum_{r \neq j} g_{rj} \gamma_r)},$$

and $\{g_{rj}\}_{rj} = G$.

One might expect to take the average over $\boldsymbol{\gamma}$ to be the assumed largest sparsity c_2 (i.e., roughly inclusion probability of each predictor),

$$\frac{1}{mp} \sum_{j=1}^{mp} \frac{1}{1 + \exp(-d - e \sum_{r \neq j} g_{rj} \gamma_r)} = c_2.$$

However, it is not easy to get an explicit or approximate expression for e via the equation above.

Our strategy is to assume at least one link/neighbour so that the parameter e is not too small. Since $\sum_{r \neq j} g_{rj} \gamma_r$ counts the number of links/neighbours of the r th feature, we let

$$\begin{aligned} \frac{1}{1 + \exp(-d - e \cdot 1)} &= c_2 \\ \Rightarrow e &= -d - \ln(c_2^{-1} - 1). \end{aligned}$$

S2: Algorithms for simulation scenarios

Algorithm 1 Simulation steps without random effects

- 1: Design a decomposable graph \mathcal{G} , $\dim(\mathcal{G}) = m \times m$
 - 2: Design a sparse matrix $\mathbf{\Gamma}$, $\dim(\mathbf{\Gamma}) = p \times m$
 - 3: Simulate $x_{ik} \sim \mathcal{N}(0, 1)$ and $x_{ik}^* \sim \mathcal{N}(0, 1)$, $i = 1, \dots, n$ and $k = 1, \dots, p$
 - 4: Simulate $\alpha_j, \beta_{kj} \sim \mathcal{N}(0, 1)$, $k = 1, \dots, p$ and $j = 1, \dots, m$
 - 5: Simulate $\tilde{u}_{ij} \sim \mathcal{N}(0, 1)$, $i = 1, \dots, n$ and $j = 1, \dots, m$
 - 6: Simulate $P \sim \mathcal{W}_{\mathcal{G}}(3, M)$ where diagonals of M are 1 and off-diagonals are 0.5, $\dim(P) = m \times m$
 - 7: Use Cholesky decomposition $\text{chol}(P^{-1})$ to get $\mathbf{U} = \tilde{\mathbf{U}} \cdot \text{chol}(P^{-1})$
 - 8: Generate $\mathbf{Y} = \mathbf{1}\alpha^\top + (\mathbf{X}\mathbf{B})_{\mathbf{\Gamma}} + \mathbf{U}$ and $\mathbf{Y}^* = \mathbf{1}\alpha^\top + \mathbf{X}^*\mathbf{B}_{\mathbf{\Gamma}} + \mathbf{U}$
-

Algorithm 2 Simulation steps with random effects

- 1: Design a decomposable graph \mathcal{G} , $\dim(\mathcal{G}) = m \times m$
 - 2: Design a sparse matrix $\mathbf{\Gamma}$, $\dim(\mathbf{\Gamma}) = p \times m$
 - Simulate $x_{ik} \sim \mathcal{N}(0, 1)$ and $x_{ik}^* \sim \mathcal{N}(0, 1)$, $i = 1, \dots, n$ and $k = 1, \dots, p$
 - 4: Simulate $\beta_{kj} \sim \mathcal{N}(0, 1)$, $k = 1, \dots, p$ and $j = 1, \dots, m$
 - Simulate $\mathbf{z}_i \sim \text{multinomial}(0.1, 0.2, 0.3, 0.4)$ and $\mathbf{z}_i^* \sim \text{multinomial}(0.1, 0.2, 0.3, 0.4)$ where $\mathbf{z}_i = (z_{i1}, \dots, z_{iT})'$, $i = 1, \dots, n$, $T = 4$
 - 6: Simulate $\beta_{0,tj} \sim \mathcal{N}(0, 2)$, $t = 1, \dots, T$ and $j = 1, \dots, m$
 - Simulate $\tilde{u}_{ij} \sim \mathcal{N}(0, 1)$, $i = 1, \dots, n$ and $j = 1, \dots, m$
 - 8: Simulate $P \sim \mathcal{W}_{\mathcal{G}}(3, M)$ where diagonals of M are 1 and off-diagonals are 0.5, $\dim(P) = m \times m$
 - Use Cholesky decomposition $\text{chol}(P^{-1})$ to get $\mathbf{U} = \tilde{\mathbf{U}} \cdot \text{chol}(P^{-1})$
 - 10: Generate $\mathbf{Y} = \mathbf{X}\mathbf{B}_{\mathbf{\Gamma}} + \mathbf{Z}\mathbf{B}_0 + \mathbf{U}$ and $\mathbf{Y}^* = \mathbf{X}^*\mathbf{B}_{\mathbf{\Gamma}} + \mathbf{Z}^*\mathbf{B}_0 + \mathbf{U}$
-

S3: Estimated \mathcal{G} for the sensitivity analysis in Section 3.3

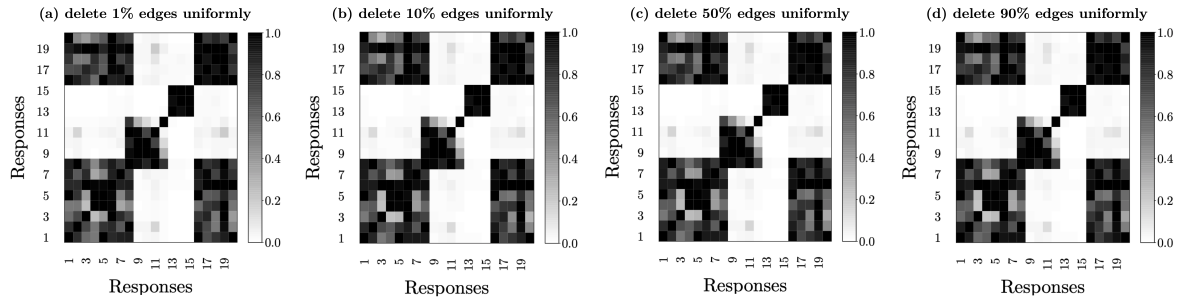


Figure S3.1: Sensitivity analysis Case 1: delete edges uniformly

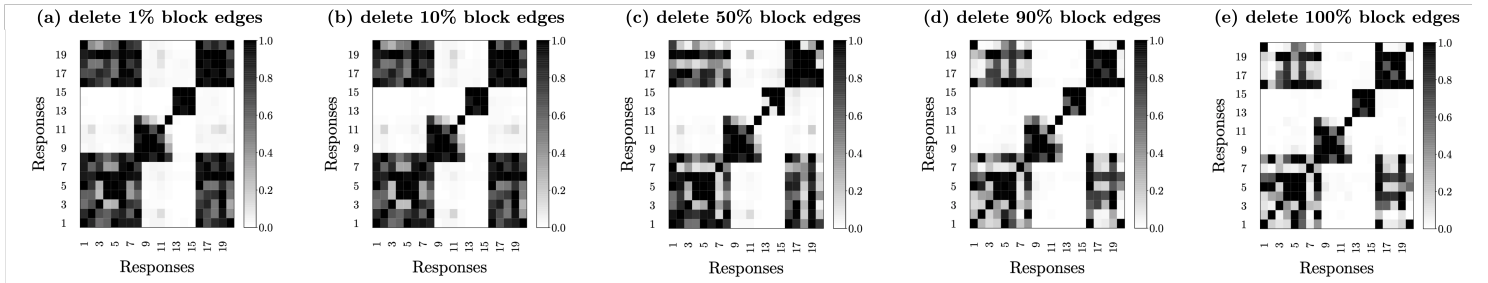


Figure S3.2: Sensitivity analysis Case 2: delete blocks of edges

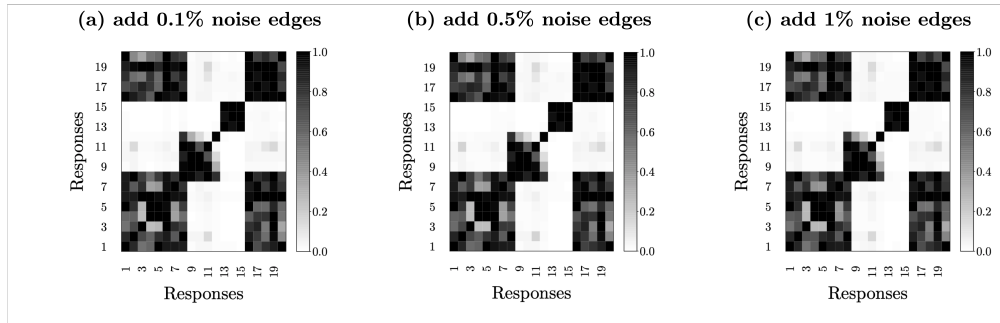


Figure S3.3: Sensitivity analysis Case 3: add noise edges

S4: More sensitivity analysis for the hyper-inverse Wishart prior

For both our approach SSUR-MRF and SSUR-hotspot, large $\nu = 100$ or a_τ in the hyper-inverse Wishart prior result in a denser $\hat{\mathcal{G}}$ (Figure S3.1, S3.3, S3.5 and S3.7). But all hyperparameters of the hyper-inverse Wishart prior are not much sensitivity to the structure recovery of $\mathbf{\Gamma}$ and response predictions (Table S3).

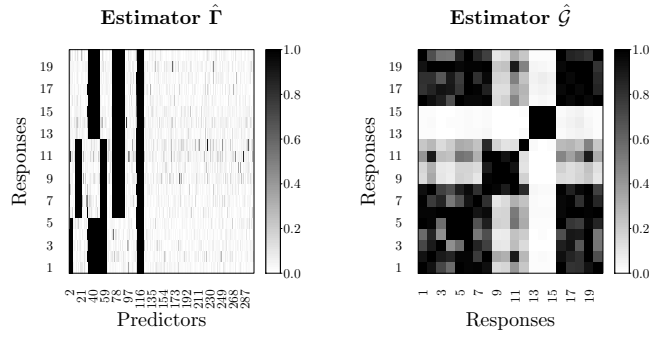


Figure S4.1: Posterior mean of the latent indicator variable $\hat{\Gamma}$ and learning structure $\hat{\mathcal{G}}$ by **SSUR-MRF**, $\mathcal{HIW}_{\mathcal{G}}(\mathbf{100}, \tau \mathbb{I})$, $\tau \sim \mathcal{Gamma}(0.1, 10)$ and $\eta \sim \mathcal{Beta}(0.1, 1)$.

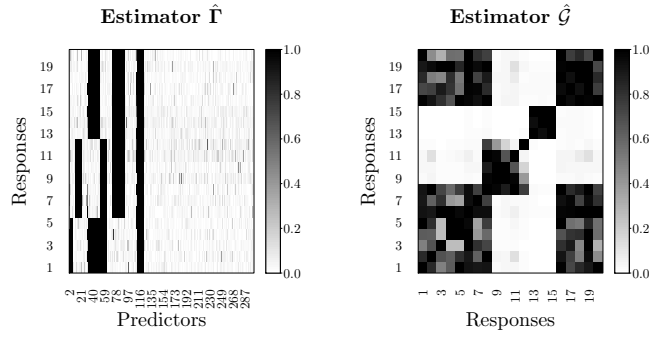


Figure S4.2: Posterior mean of the latent indicator variable $\hat{\Gamma}$ and learning structure $\hat{\mathcal{G}}$ by **SSUR-MRF** $\mathcal{HIW}_{\mathcal{G}}(22, \tau \mathbb{I})$, $\tau \sim \mathcal{Gamma}(\mathbf{0.001}, 10)$ and $\eta \sim \mathcal{Beta}(0.1, 1)$.

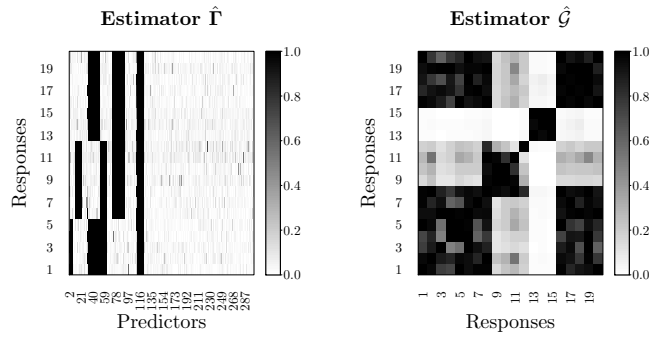


Figure S4.3: Posterior mean of the latent indicator variable $\hat{\Gamma}$ and learning structure $\hat{\mathcal{G}}$ by **SSUR-MRF**, $\mathcal{HIW}_{\mathcal{G}}(22, \tau \mathbb{I})$, $\tau \sim \mathcal{Gamma}(\mathbf{100}, 10)$ and $\eta \sim \mathcal{Beta}(0.1, 1)$.

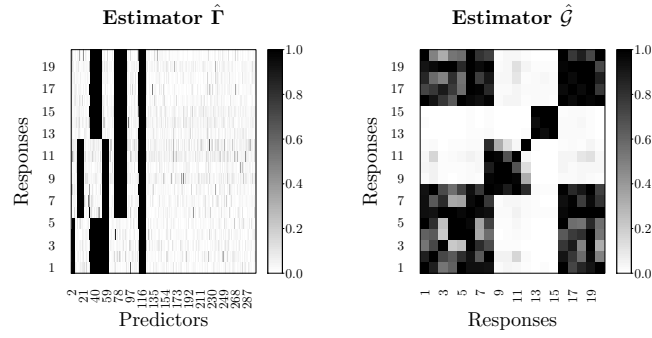


Figure S4.4: Posterior mean of the latent indicator variable $\hat{\Gamma}$ and learning structure $\hat{\mathcal{G}}$ by **SSUR-MRF**, $\mathcal{H}\mathcal{I}\mathcal{W}_{\mathcal{G}}(22, \tau\mathbb{I})$, $\tau \sim \mathcal{Gamma}(0.1, 10)$ and $\eta \sim \mathcal{Beta}(\mathbf{0.001}, 1)$.

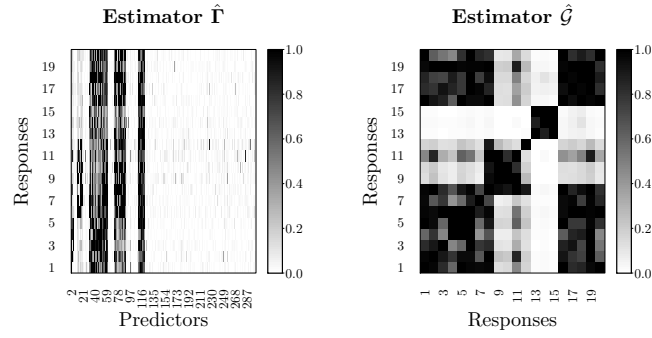


Figure S4.5: Posterior mean of the latent indicator variable $\hat{\Gamma}$ and learning structure $\hat{\mathcal{G}}$ by **SSUR-hotspot** prior, $\mathcal{H}\mathcal{I}\mathcal{W}_{\mathcal{G}}(\mathbf{100}, \tau\mathbb{I})$, $\tau \sim \mathcal{Gamma}(0.1, 10)$ and $\eta \sim \mathcal{Beta}(0.1, 1)$.

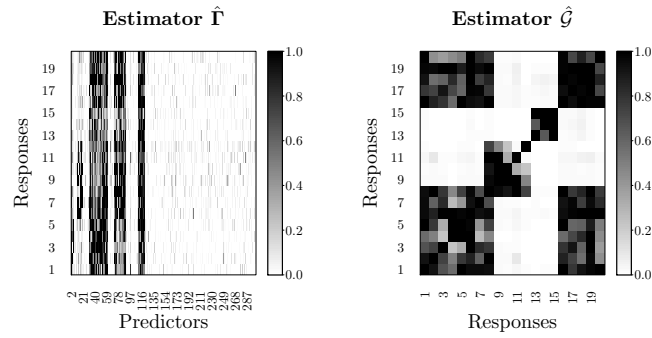


Figure S4.6: Posterior mean of the latent indicator variable $\hat{\Gamma}$ and learning structure $\hat{\mathcal{G}}$ by **SSUR-hotspot** prior, $\mathcal{H}\mathcal{I}\mathcal{W}_{\mathcal{G}}(22, \tau\mathbb{I})$, $\tau \sim \mathcal{Gamma}(\mathbf{0.001}, 10)$ and $\eta \sim \mathcal{Beta}(0.1, 1)$.

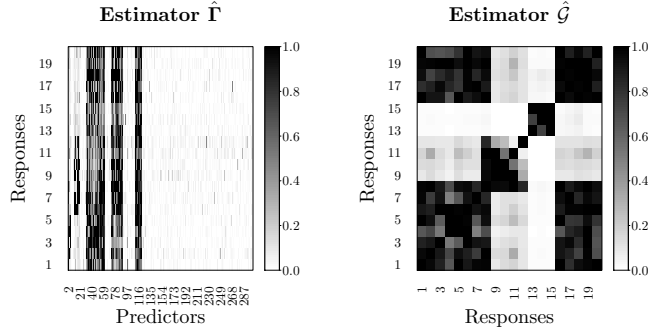


Figure S4.7: Posterior mean of the latent indicator variable $\hat{\Gamma}$ and learning structure $\hat{\mathcal{G}}$ by **SSUR-hotspot** prior, $\mathcal{HW}_{\mathcal{G}}(22, \tau\mathbb{I})$, $\tau \sim \text{Gamma}(100, 10)$ and $\eta \sim \text{Beta}(0.1, 1)$.

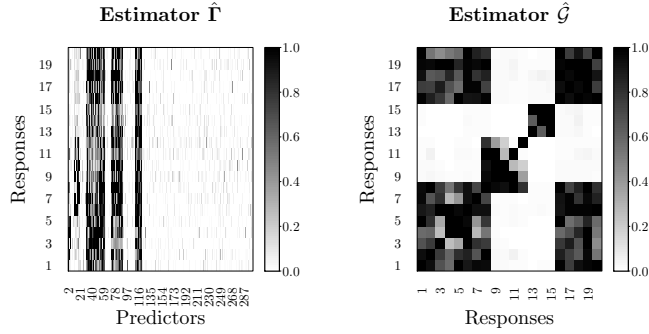


Figure S4.8: Posterior mean of the latent indicator variable $\hat{\Gamma}$ and learning structure $\hat{\mathcal{G}}$ by **SSUR-hotspot** prior, $\mathcal{HW}_{\mathcal{G}}(22, \tau\mathbb{I})$, $\tau \sim \text{Gamma}(0.1, 10)$ and $\eta \sim \text{Beta}(0.001, 1)$.

Table S4: Performance of variable selection and response predictions by SSUR-MRF and SSUR-hotspot with different hyper-inverse Wishart prior

	accuracy	sensitivity	specificity	$\widehat{\text{elpd}}_{\text{loo}}$	$\widehat{\text{elpd}}_{\text{waic}}$	RMSE	RMSPE
SSUR-MRF							
$\nu = 22, \tau \sim \text{Gamma}(0.1, 10), \eta \sim \text{Beta}(0.1, 1)^\dagger$	0.982	0.971	0.984	-21044.6	-21045.3	13.860	7.167
$\nu = 100, \tau \sim \text{Gamma}(0.1, 10), \eta \sim \text{Beta}(0.1, 1)$	0.981	0.969	0.983	-21068.5	-21069.6	13.718	7.098
$\nu = 22, \tau \sim \text{Gamma}(0.001, 10), \eta \sim \text{Beta}(0.1, 1)$	0.982	0.970	0.984	-21044.4	-21045.1	13.838	7.149
$\nu = 22, \tau \sim \text{Gamma}(100, 10), \eta \sim \text{Beta}(0.1, 1)$	0.982	0.967	0.985	-21044.4	-21045.2	13.853	7.181
$\nu = 22, \tau \sim \text{Gamma}(0.1, 10), \eta \sim \text{Beta}(0.001, 1)$	0.982	0.971	0.984	-21044.1	-21045.0	13.838	7.149
SSUR-hotspot							
$\nu = 22, \tau \sim \text{Gamma}(0.1, 10), \eta \sim \text{Beta}(0.1, 1)^\dagger$	0.931	0.753	0.968	-21045.2	-21045.7	14.135	7.971
$\nu = 100, \tau \sim \text{Gamma}(0.1, 10), \eta \sim \text{Beta}(0.1, 1)$	0.929	0.770	0.964	-21068.6	-21069.6	13.875	7.765
$\nu = 22, \tau \sim \text{Gamma}(0.001, 10), \eta \sim \text{Beta}(0.1, 1)$	0.932	0.767	0.966	-21024.8	-21027.5	14.156	7.963
$\nu = 22, \tau \sim \text{Gamma}(100, 10), \eta \sim \text{Beta}(0.1, 1)$	0.933	0.770	0.967	-21044.3	-21045.0	14.137	7.827
$\nu = 22, \tau \sim \text{Gamma}(0.1, 10), \eta \sim \text{Beta}(0.001, 1)$	0.933	0.739	0.968	-21036.2	-21037.4	14.185	8.020

[†]These specifications are the same as the SSUR models in Table 1.

S5: MCMC diagnostics by SSUR-Ber and SSUR-MRF in the GDSC data analysis

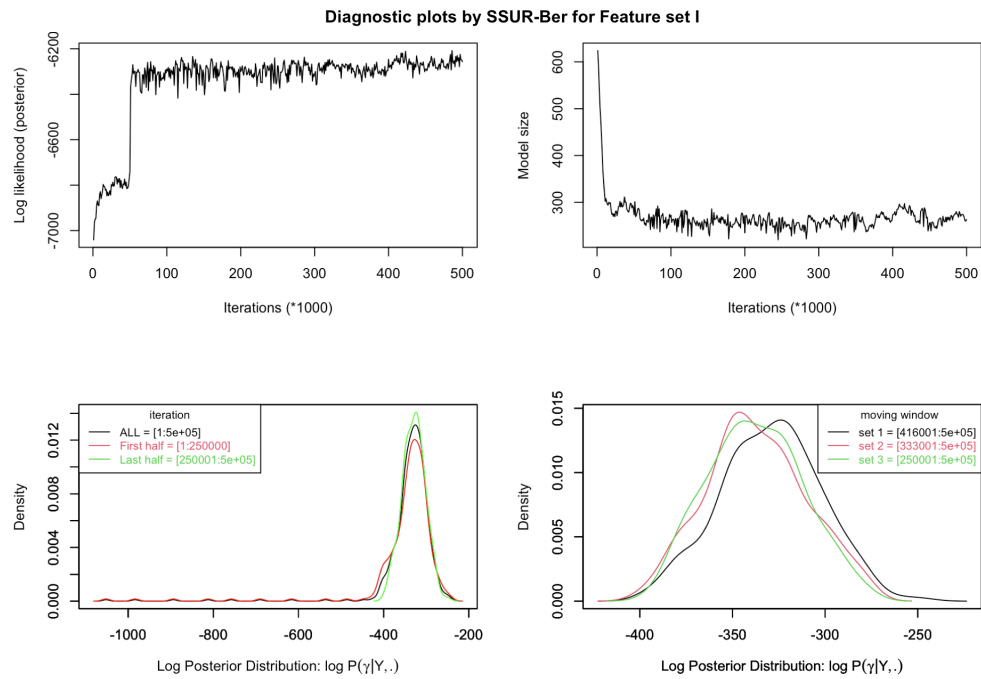


Figure S5.1.1: Diagnostic plots of the MCMC sampler with 6 chains, 500 000 iterations and a burn-in of 300 000 iterations. The hyperparameters set `hyperpar = list(mrf_d=-2, mrf_e=0, a_w0=55, b_w0=400, a_w=4, b_w=32)`, and others are by default.

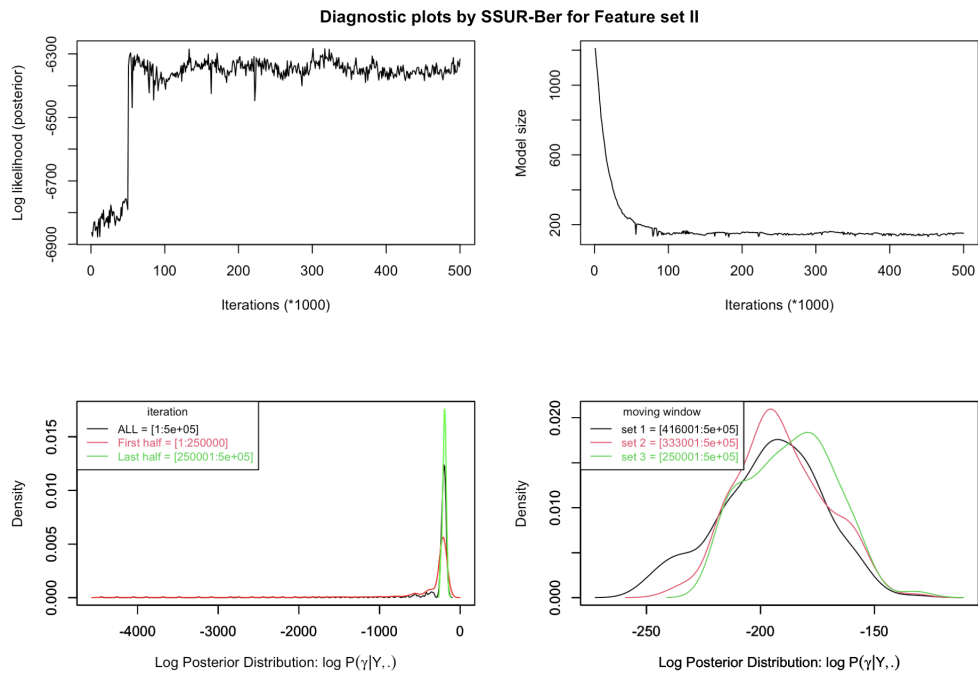


Figure S5.1.2: Diagnostic plots of the MCMC sampler with 8 chains, 500 000 iterations and a burn-in of 300 000 iterations. The hyperparameters set `hyperpar = list(mrf_d=-4, mrf_e=0, a_w0=55, b_w0=400, a_w=4, b_w=32)`, and others are by default.

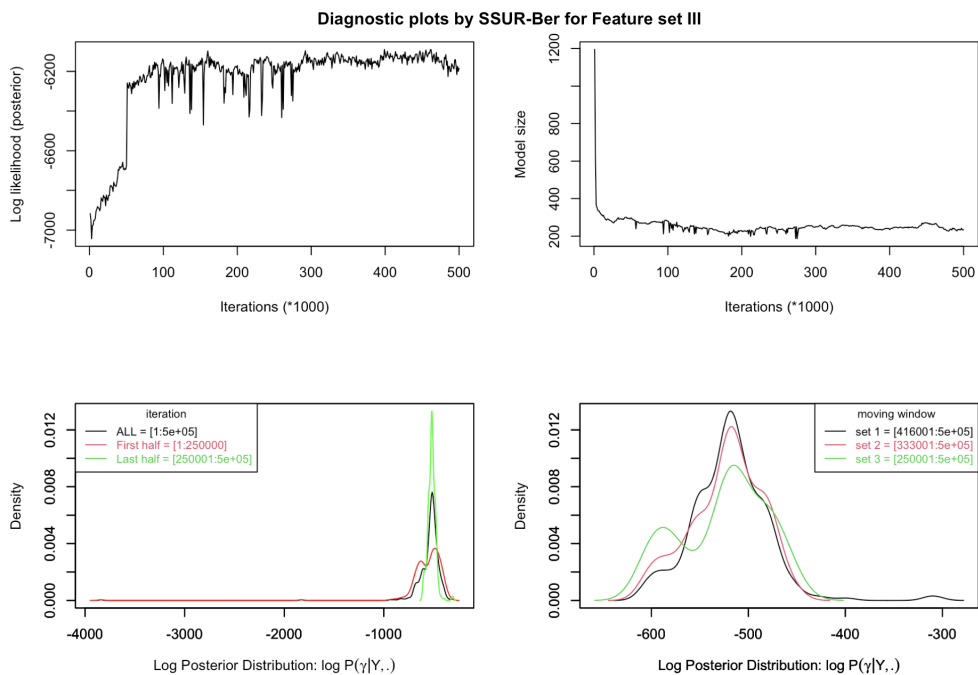


Figure S5.1.3: Diagnostic plots of the MCMC sampler with 11 chains, 500 000 iterations and a burn-in of 300 000 iterations. The hyperparameters set `hyperpar = list(mrf_d=-3.5, mrf_e=0, a_w0=55, b_w0=400, a_w=4, b_w=33)`, and others are by default.

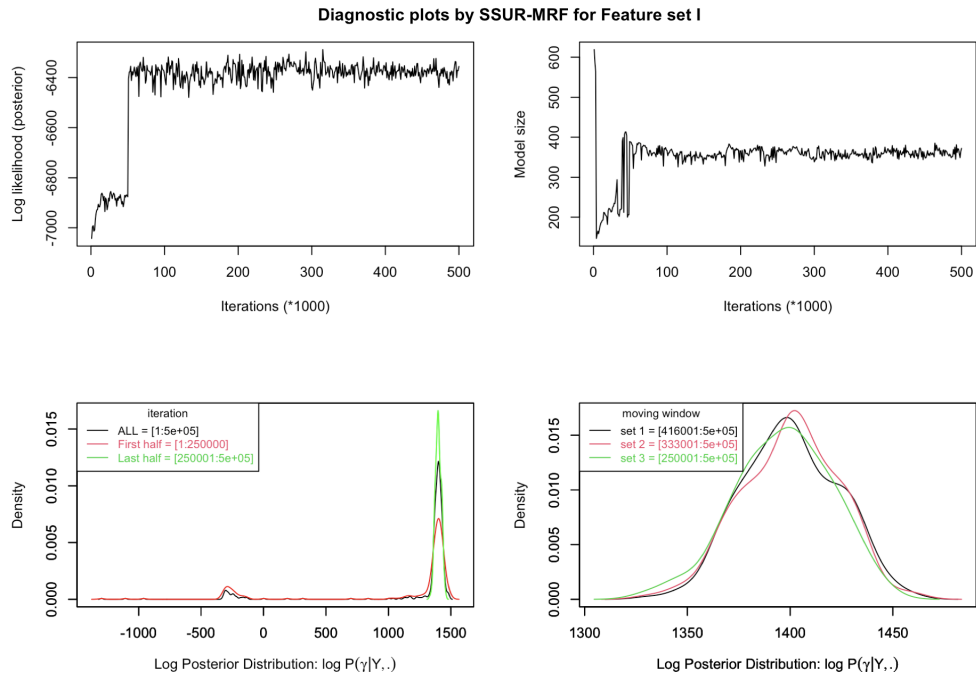


Figure S5.2.1: Diagnostic plots of the MCMC sampler with 6 chains, 500 000 iterations and a burn-in of 300 000 iterations. The hyperparameters set `hyperpar = list(mrf_d=-2, mrf_e=0, a_w0=55, b_w0=400, a_w=4, b_w=32)`, and others are by default.

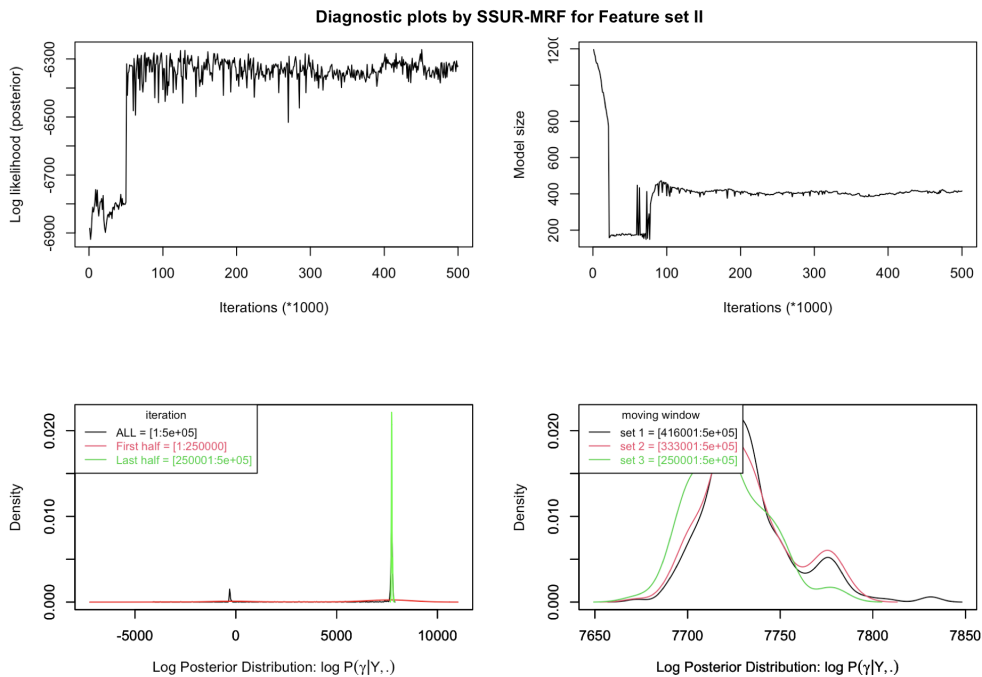


Figure S5.2.2: Diagnostic plots of the MCMC sampler with 8 chains, 500 000 iterations and a burn-in of 300 000 iterations. The hyperparameters set `hyperpar = list(mrf_d=-4, mrf_e=0.3, a_w0=55, b_w0=400, a_w=4, b_w=32)`, and others are by default.

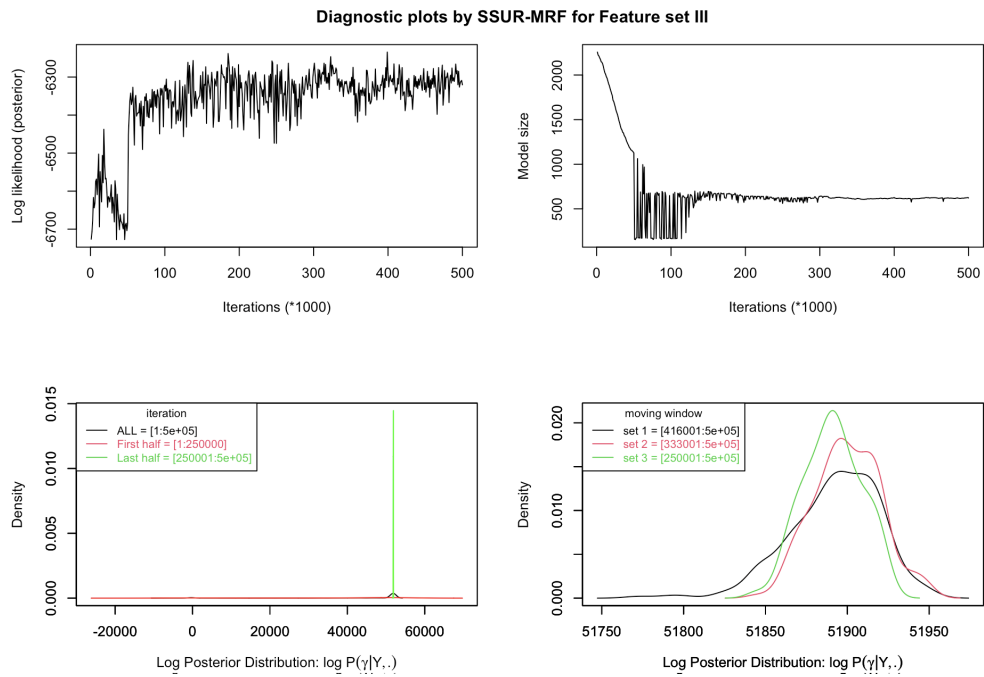


Figure S5.2.3: Diagnostic plots of the MCMC sampler with 8 chains, 500 000 iterations and a burn-in of 300 000 iterations. The hyperparameters set `hyperpar = list(mrf_d=-4.6, mrf_e=0.5, a_w0=55, b_w0=400, a_w=4, b_w=33)`, and others are by default.

S6: Estimated residual structure between the seven drugs in the GDSC data analysis

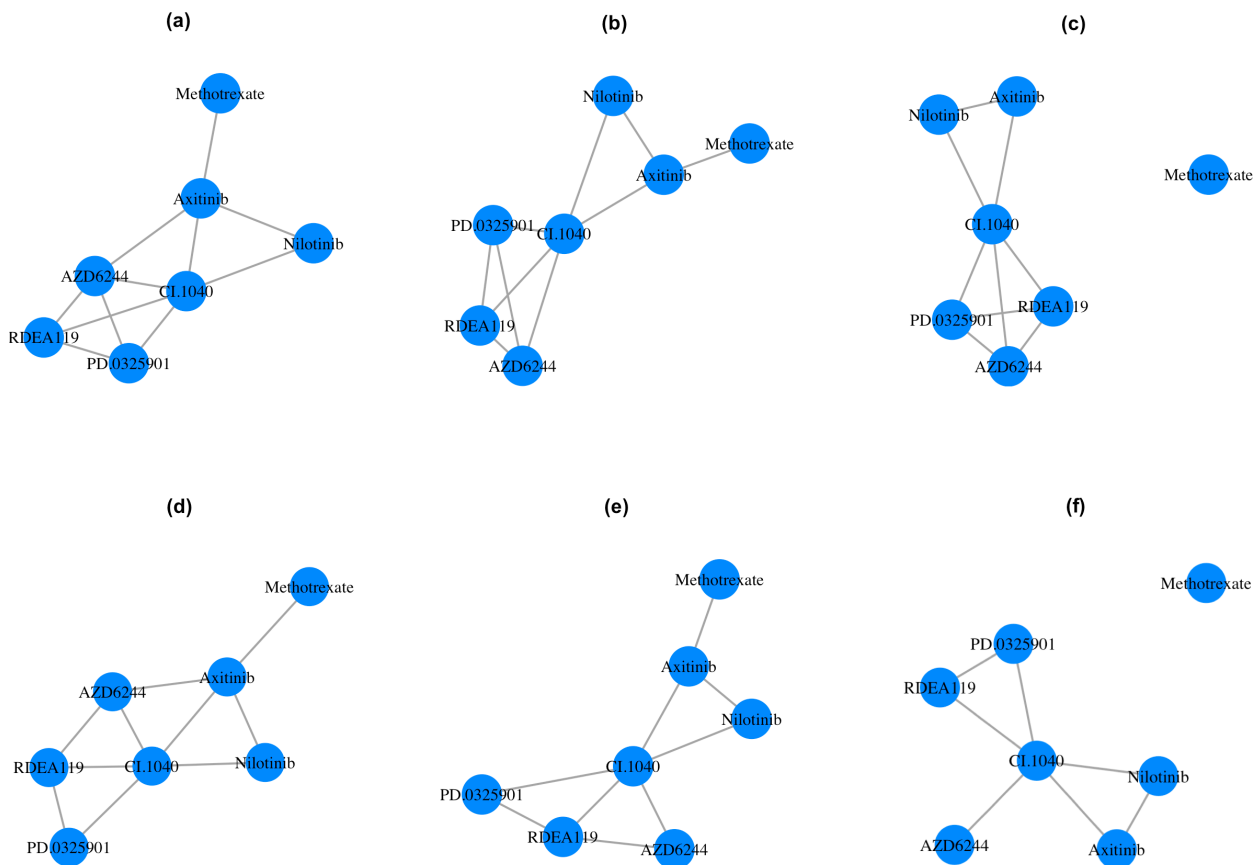


Figure S6: Estimated residual structure between the seven drugs by SSUR-MRF and SSUR-Ber based on \hat{G} thresholded at 0.5. Panels (a)-(c) are estimated by SSUR-MRF, and panels (d)-(f) are estimated by SSUR-Ber, corresponding to Feature sets I, II and III respectively

S7: Identified genomic features for the MAPK inhibitors by SSUR-Ber in the GDSC data analysis

Table S7.1 GDSC data application: Identified genomic features for the MAPK inhibitors by SSUR-Ber

	Identified genomic features
Feature set I	ABCC3; LXN; LGALS3.GALIG; MAGED4.LOC653210; ZNF198.CNV
Feature set II	IGFBP6; CA14; C10RF115; LAMC2; TIMP1
Feature set III	ATF5; FAAH; ABCB4; IGFBP6; IGFBP2; CENTD3; MAST4; MITF; FGR; CA14; PYGL; MEIS1; LAMC2; SPINK1; CRISPLD2; FLT3; P2RY10; ZNF204; GRAMD3; ELMO1; LIFR; ALDH3B1; SPRY2; S100A11; KCTD12; PBX1.CNV; FBXW7.MUT; BCR.ABL.MUT

Table S7.2 GDSC data application: Identified common features across feature sets I, II, and III for the MAPK inhibitors by SSUR-MRF.

Identified common features
AKT2.CNV; ALK.CNV; BRCA1.CNV; DDX10.CNV; EIF4A2.CNV; ELL.CNV; FGFR10P.CNV; FGFR3.CNV; FH.CNV; IDH1.CNV; KTN1.CNV; MDM2.CNV; MYCL1.CNV; NF2.CNV; NIN.CNV; NSD1.CNV; NTRK3.CNV; PDGFRA.CNV; PDGFRB.CNV; PER1.CNV; RANBP17.CNV; TPM3.CNV; ALK.MUT; BRCA1.MUT; EP300.MUT; FGFR3.MUT; FLCN.MUT; IDH1.MUT; MAP2K4.MUT; MDM2.MUT; MYCL1.MUT; NF2.MUT; PDGFRA.MUT; PIK3CA.MUT; TSC1.MUT

NOTE: Gene RANBP17.CNV is not in the Cancer Gene Census database.

Table S7.3 GDSC data application: Identified features by Feature set III but not identified by Feature set I or II for the MAPK inhibitors by SSUR-MRF.

Identified features by Feature set III but not identified by Feature set I or II
PLEKHB1; PTPRU; RGC32; ARNT2; SLC30A3; PTPN6; SNTG2; IL1R1; PLTP; TRPS1; CCND2; EFS; PTK2B; MMP9; GNG7; CA14; BCAR3; ZNF532; HSPA6; TMEM45A; DUSP4; DUSP2; DUSP1; HPGD; IL18; IL24; NRTN; FGFR3; TRDV2; USH1C; CDO1; TIAM1; ATP2A3; NLGN1; LOC284244; FLJ14082; LGALS3; CYP26A1; BCL2; RASGRP1; RASGRP2; SYNPO; RORA; TRAC; KRT6B; ACTN1; ZFP30; PRKCB1; PDGFRB; HOXA10; KHDRBS3; RIBC2; LCN2; TSPY1; CDC42EP1; MYH10; WIF1; CCND2.CNV; KRAS.CNV; CCND2.MUT; KDM5C.MUT

S8: Prediction performance for Feature sets I, II and III in the GDSC data analysis

Table S8 GDSC data application: Similar prediction performance between the SSUR-Ber and SSUR-MRF models.

	SSUR-Ber	SSUR-MRF
Feature set I		
elpd.LOO	-8190	-8162
elpd.WAIC	-8219	-8212
RMSE	2.116	2.133
RMSPE	2.110	2.097
Feature set II		
elpd.LOO	-8135	-8140
elpd.WAIC	-8136	-8139
RMSE	1.866	1.810
RMSPE	1.810	1.972
Feature set III		
elpd.LOO	-8136	-8143
elpd.WAIC	-8169	-8178
RMSE	2.003	1.883
RMSPE	2.095	2.062

S9: Drug responses across cancer tissue types for each drug

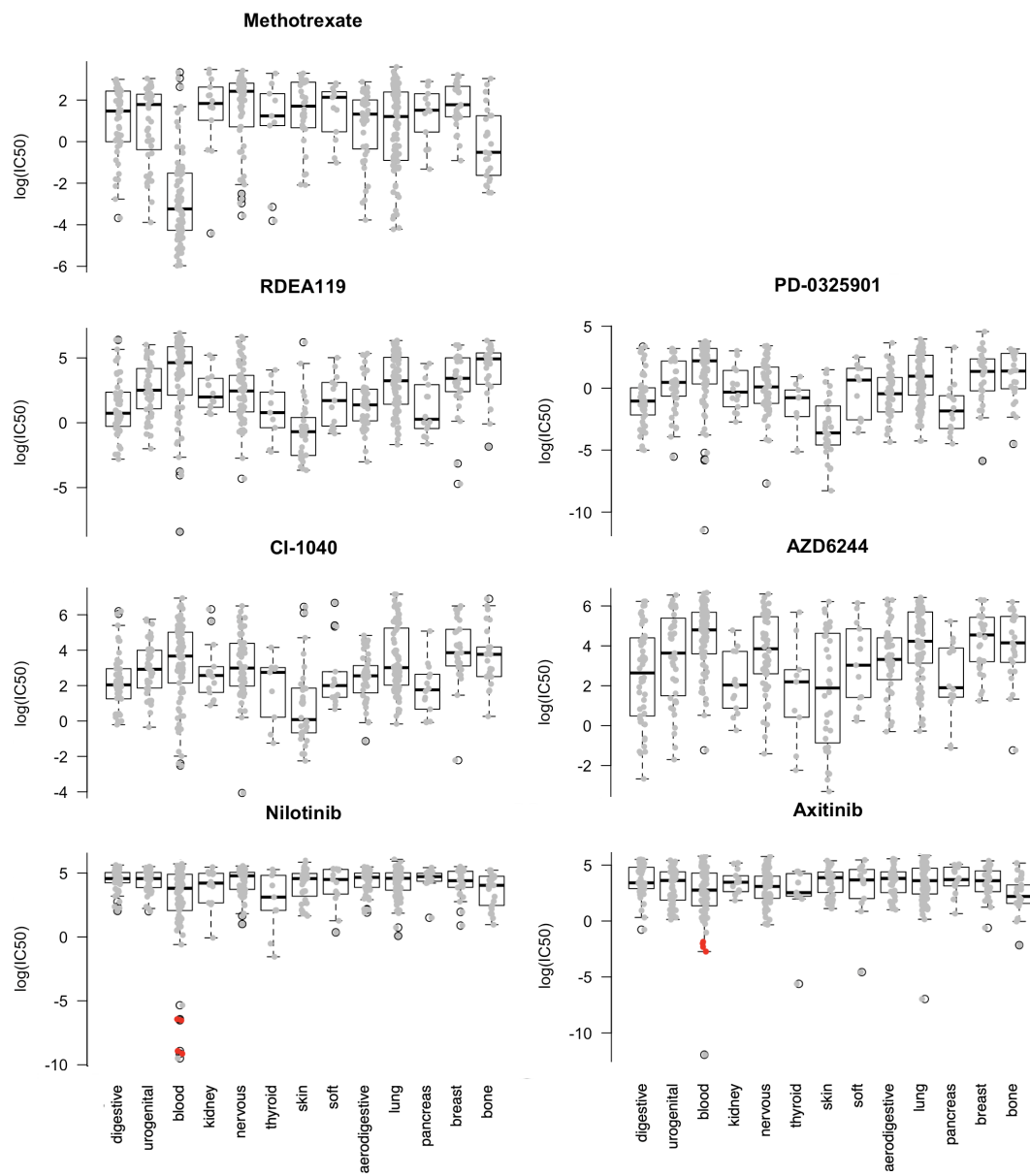


Figure S9 GDSC data application: Drug responses across cancer tissue types for each drug. Each grey dot corresponds each cancer cell line. Red points “•” correspond to the BCR-ABL mutated blood cell lines treated by drugs Nilotinib and Axitinib.